

**Measurement of the b Quark Fragmentation
Function in Z^0 decays
and First Measurement of $B - \bar{B}$ Energy Correlations***

The SLD Collaboration**

Stanford Linear Accelerator Center
Stanford University, Stanford, CA 94309

ABSTRACT

We present preliminary results of a new measurement of the inclusive b quark fragmentation function in Z^0 decays using a novel kinematic B hadron energy reconstruction technique. The measurement is performed using 350,000 hadronic Z^0 events recorded in the SLD experiment at SLAC between 1997 and 1998. The small and stable SLC beam spot and the CCD-based vertex detector are used to reconstruct topological B -decay vertices with high efficiency and purity, and to provide precise measurements of the kinematic quantities used in this technique. We measure the B energy with good efficiency and resolution over the full kinematic range. We compare the measured scaled B hadron energy distribution with several functional forms of the B hadron energy distribution and predictions of several models of b quark fragmentation. Several functions are excluded by the data. The average scaled energy of the weakly decaying B hadron is measured to be $x_B = 0.710 \pm 0.003$ (stat) ± 0.005 (syst) ± 0.004 (model) (preliminary). In addition, we reconstruct the decay vertices of both the leading B and \bar{B} hadrons in a large sample of events, and measure their energies. We present the first (preliminary) measurement of the correlation between the B and \bar{B} energies in $Z^0 \rightarrow b\bar{b}$ events, and compare with the leading order QCD prediction.

Contributed to: the International Europhysics Conference on High Energy Physics, 12–18 July, 2001, Budapest, Hungary, Refs: 666 and 673; and the XXth International Symposium on Lepton and Photon Interactions, 23–28 July, 2001, Rome, Italy.

* Work supported by Department of Energy contract DE-AC03-76SF00515 (SLAC).

1 Introduction

The production of heavy hadrons (H) in e^+e^- annihilation provides a laboratory for the study of heavy-quark (Q) jet fragmentation. This is commonly characterised in terms of the observable $x_H \equiv 2E_H/\sqrt{s}$, where E_H is the energy of a B or D hadron containing a b or c quark, respectively, and \sqrt{s} is the c.m. energy. In contrast to light-quark jet fragmentation one expects [1] the distribution of x_H , $D(x_H)$, to peak at an x_H -value significantly above 0. Since the hadronisation process is intrinsically non-perturbative $D(x_H)$ cannot be calculated directly using perturbative Quantum Chromodynamics (QCD). However, the distribution of the closely-related variable $x_Q \equiv 2E_Q/\sqrt{s}$ can be calculated perturbatively [2, 3, 4] and related, via model-dependent assumptions, to the observable quantity $D(x_H)$; a number of such models of heavy quark fragmentation have been proposed [5, 6, 7]. Measurements of $D(x_H)$ thus serve to constrain both perturbative QCD and the model predictions. Furthermore, the measurement of $D(x_H)$ at different c.m. energies can be used to test QCD evolution, and comparison of $D(x_B)$ with $D(x_D)$ can be used to test heavy quark symmetry [8, 9]. Finally, the uncertainty on the forms of $D(x_D)$ and $D(x_B)$ must be taken into account in studies of the production and decay of heavy quarks, see *eg.* [10]; more accurate measurements of these forms will allow increased precision in tests of the electroweak heavy-quark sector.

We consider the measurement of the B hadron scaled energy distribution $D(x_B)$ in Z^0 decays. Earlier studies [11] used the momentum spectrum of the lepton from semi-leptonic B decays to constrain the mean value $\langle x_B \rangle$ and found it to be approximately 0.70; this is in agreement with the results of similar studies at $\sqrt{s} = 29$ and 35 GeV [12]. In more recent analyses [13, 14, 15] the scaled energy distribution $D(x_B)$ has been measured by reconstructing B hadrons via their $B \rightarrow D\ell X$ decay mode. In this case the reconstruction efficiency is intrinsically low due to the small branching ratio for B hadrons to decay into the high-momentum leptons used in the tag. Also, the reconstruction of the B hadron energy using calorimeter information usually has poor resolution for low B energy, resulting in poor sensitivity to the shape of the distribution at low energy.

Here we describe the preliminary results of a new method for reconstructing B hadron decays, and the B energy, inclusively, using only charged tracks, in the SLD experiment at SLAC. We use the upgraded CCD vertex detector, installed in 1996, to reconstruct B -decay vertices with high efficiency and purity. Combined with the micron-size SLC interaction point (IP), precise vertexing allows us to reconstruct accurately the B flight direction and hence the transverse momentum of tracks associated with the vertex with respect to this direction. Using the transverse momentum and the total invariant mass of the associated tracks, an upper limit on the mass of the missing particles is found for each reconstructed B -decay vertex, and is used to solve for the longitudinal momentum of the missing particles, and hence for the energy of the B hadron. In order to improve the B sample purity and the reconstructed B hadron energy resolution, B vertices with low missing mass are selected. The method is described in Section 3. In Section 4

we compare the B energy distribution with predictions of heavy quark fragmentation models. We also test several functional forms of B hadron energy distributions. In Section 5, we unfolded the B hadron energy distribution. In Section 6, we discuss the systematic errors.

We have also studied events in which we reconstructed the energies of both leading B hadrons produced via $e^+e^- \rightarrow b\bar{b} \rightarrow B\bar{B} + X$. As proposed in [16], we have measured moments of the correlated scaled-energy distribution $d^2N/dx_{B1}dx_{B2}$:

$$D_{ij} \equiv \int \int x_{B1}^i x_{B2}^j d^2N/(dx_{B1}dx_{B2}) dx_{B1}dx_{B2},$$

where x_{B1} and x_{B2} are the scaled energies of the two B hadrons, and the label is arbitrary. By comparing these with the moments of the single inclusive distribution $D(x_B)$:

$$D_i \equiv \int x_B^i dN/dx_B dx_B$$

we have tested the ansatz of factorization as applied to pQCD calculations of $e^+e^- \rightarrow b\bar{b}(g)$ events. This analysis is described in Section 7. In Section 8 we summarize the results.

2 Apparatus and Hadronic Event Selection

This analysis is based on roughly 350,000 hadronic events produced in e^+e^- annihilations at a mean center-of-mass energy of $\sqrt{s} = 91.28$ GeV at the SLAC Linear Collider (SLC), and recorded in the SLC Large Detector (SLD) in 1997 and 1998. A general description of the SLD can be found elsewhere [17]. The trigger and initial selection criteria for hadronic Z^0 decays are described in Ref. [18]. This analysis used charged tracks measured in the Central Drift Chamber (CDC) [19] and in the upgraded Vertex Detector (VXD3) [20]. Momentum measurement is provided by a uniform axial magnetic field of 0.6T. The CDC and VXD3 give a momentum resolution of $\sigma_{p_\perp}/p_\perp = 0.01 \oplus 0.0026p_\perp$, where p_\perp is the track momentum transverse to the beam axis in GeV/c. In the plane normal to the beamline the centroid of the micron-sized SLC IP is reconstructed from tracks in sets of approximately thirty sequential hadronic Z^0 decays to a precision of $\sigma^{r\phi} \simeq 4 \pm 2 \mu\text{m}$. The IP position along the beam axis is determined event by event using charged tracks with a resolution of $\sigma^z \simeq 20 \mu\text{m}$. Including the uncertainty on the IP position, the resolution on the charged-track impact parameter (d) projected in the plane perpendicular to the beamline is $\sigma_d^{r\phi} = 8 \oplus 33/(p \sin^{3/2} \theta) \mu\text{m}$, and the resolution in the plane containing the beam axis is $\sigma_d^z = 10 \oplus 33/(p \sin^{3/2} \theta) \mu\text{m}$, where θ is the track polar angle with respect to the beamline. The event thrust axis [21] is calculated using energy clusters measured in the Liquid Argon Calorimeter [22].

A set of cuts is applied to the data to select well-measured tracks and events well contained within the detector acceptance. Charged tracks are required to have a distance of closest approach transverse to the beam axis within 5 cm, and within 10 cm along the axis from the measured IP, as well as $|\cos \theta| < 0.80$, and $p_\perp > 0.15$ GeV/c. Events

are required to have a minimum of seven such tracks, a thrust axis polar angle w.r.t. the beamline, θ_T , within $|\cos \theta_T| < 0.71$, and a charged visible energy E_{vis} of at least 20 GeV, which is calculated from the selected tracks assigned the charged pion mass. The efficiency for selecting a well-contained $Z^0 \rightarrow q\bar{q}(g)$ event is estimated to be above 96% independent of quark flavor. The selected sample comprised 218,953 events, with an estimated $0.10 \pm 0.05\%$ background contribution dominated by $Z^0 \rightarrow \tau^+\tau^-$ events.

For the purpose of estimating the efficiency and purity of the B hadron selection procedure we made use of a detailed Monte Carlo (MC) simulation of the detector. The JETSET 7.4 [23] event generator is used, with parameter values tuned to hadronic e^+e^- annihilation data [24], combined with a simulation of B hadron decays tuned [25] to $\Upsilon(4S)$ data and a simulation of the SLD based on GEANT 3.21 [26]. Inclusive distributions of single-particle and event-topology observables in hadronic events are found to be well described by the simulation [18]. Uncertainties in the simulation are taken into account in the systematic errors (Section 6).

3 B Hadron Selection and Energy Measurement

3.1 B Hadron Selection

The B sample for this analysis is selected using a topological vertexing technique based on the detection and measurement of charged tracks, which is described in detail in Ref. [27]. Each hadronic event is divided into two hemispheres by a plane perpendicular to the thrust axis. In each hemisphere the topological vertexing algorithm is applied to the set of ‘quality’ tracks having (i) at least 23 hits in the CDC and 2 hits in VXD3; (ii) a combined CDC and VXD3 track fit quality of $\chi^2/N_{dof} < 8$; (iii) a momentum in the range $0.25 < p < 55$ GeV/ c , (iv) an impact parameter of less than 0.3 cm in the $r\phi$ plane, and less than 1.5 cm along the z axis; (v) a transverse impact parameter error no larger than 250 μm .

Vertices consistent with photon conversions or K^0 and Λ^0 decays are discarded. In hemispheres containing at least one found vertex the vertex furthest from the IP is retained as the ‘seed’ vertex. Those events are retained which contain a seed vertex separated from the IP by between 0.1 cm and 2.3 cm. The lower bound reduces contamination from non- B -decay tracks and backgrounds from light-flavor events, and the upper bound reduces the background from particle interactions with the beam pipe.

For each hemisphere containing an accepted seed vertex, a vertex axis is formed by the straight line joining the IP to the seed vertex, which is located at a distance D from the IP. For each quality track not directly associated with the vertex, the distance of closest approach to the vertex axis, T , and the distance from the IP along the vertex axis to the point of closest approach, L , are calculated. Tracks satisfying $T < 1$ mm and $L/D > 0.3$ are added to the vertex. These T and L cuts are chosen to minimize false track associations to the seed vertex, since typically the addition of a false track has a much greater kinematic effect than the omission of a genuine B -decay track, and hence

has more effect on the reconstructed B hadron energy resolution. Our Monte Carlo studies show that, on average, this procedure attaches 0.85 tracks to each seed vertex, 91.9% of the tracks from tagged true B decays are associated with the resulting vertices, and 98.0% of the vertex tracks are from true B decays.

The large masses of the B hadrons relative to light-flavor hadrons make it possible to distinguish B hadron decay vertices from those vertices found in events of light flavors using the vertex invariant mass, M . However, due to the missing particles, which are mainly neutrals, M cannot be fully determined. In the *rest* frame of the decaying hadron, M can be written as

$$M = \sqrt{M_{ch}^2 + P_t^2 + P_{chl}^2} + \sqrt{M_0^2 + P_t^2 + P_{0l}^2} \quad (1)$$

where M_{ch} and M_0 are the total invariant masses of the set of vertex-associated tracks and the set of missing particles, respectively. P_t is the total charged track momentum transverse to the B flight direction, which is identical to the transverse momentum of the set of missing particles by momentum conservation. P_{chl} and P_{0l} are the respective momenta along the B flight direction. In the B *rest* frame, $P_{chl} = P_{0l}$. Using the set of vertex-associated charged tracks, we calculate the total momentum vector \vec{P}_{ch} and its component transverse to the flight direction P_t , and the total energy E_{ch} and invariant mass M_{ch} , assuming the charged pion mass for each track. The lower bound for the mass of the decaying hadron, the ‘ P_t -corrected vertex mass’,

$$M_{Pt} = \sqrt{M_{ch}^2 + P_t^2} + |P_t| \quad (2)$$

is used as the variable for selecting B hadrons. The majority of non- B vertices have M_{Pt} less than 2.0 GeV/ c^2 . However, occasionally the measured P_t may fluctuate to a much larger value than the true P_t , causing some charm vertices to have a M_{Pt} larger than 2.0 GeV/ c^2 . To reduce this contamination, we calculate the ‘minimum P_t ’ by allowing the locations of the IP and the vertex to float to any pair of locations within the respective one sigma error-ellipsoids, We substitute the minimum P_t in Equation (2) and use the modified M_{Pt} as our variable for selecting B hadrons [28].

Figure 1 shows the distribution of the M_{Pt} for the 76,421 hemispheres in the data sample with a found secondary vertex, and the corresponding simulated distribution (histogram). B hadron candidates are selected by requiring $M_{Pt} > 2.0$ GeV/ c^2 . We further required $M_{Pt} \leq 2 \times M_{ch}$ to reduce the contamination from fake vertices in light quark events [28]. A total of 42,093 hemispheres are selected, with an estimated efficiency for selecting a true B -hemisphere of 43.7%, and a sample purity of 98.2%. The contributions from light-flavor events in the sample are 0.34% for primary u,d and s events and 1.47% for c events.

3.2 B Hadron Energy Measurement

The energy of each B hadron, E_B , can be expressed as the sum of the reconstructed-vertex energy, E_{ch} , and the energy of those particles not associated with the vertex, E_0 .

We can write E_0 as

$$E_0^2 = M_0^2 + P_t^2 + P_{0l}^2 \quad (3)$$

The two unknowns, M_0 and P_{0l} , must be found in order to obtain E_0 . One kinematic constraint can be obtained by imposing the B hadron mass on the vertex, $M_B^2 = E_B^2 - P_B^2$, where $P_B = P_{chl} + P_{0l}$ is the total momentum of the B hadron, and P_{chl} is the momentum component of the vertex-associated tracks along the vertex axis. From Equation (1) we derive the following inequality,

$$\sqrt{M_{ch}^2 + P_t^2} + \sqrt{M_0^2 + P_t^2} \leq M_B, \quad (4)$$

where equality holds in the limit where both P_{0l} and P_{chl} vanish in the B hadron *rest* frame. Equation (4) effectively sets an upper bound on M_0 , and a lower bound is given by zero:

$$0 \leq M_0^2 \leq M_{0max}^2, \quad (5)$$

where

$$M_{0max}^2 = M_B^2 - 2M_B\sqrt{M_{ch}^2 + P_t^2} + M_{ch}^2. \quad (6)$$

Since M_0 is bounded from both above and below, we expect to obtain a good estimate of M_0 , and therefore of the B hadron energy, when M_{0max}^2 is small.

We have used our simulation to study this issue. Assuming $M_B = 5.28 \text{ GeV}/c^2$, the true value of M_0 tends to cluster near its maximum value M_{0max} . Figure 2 shows the relative deviation of M_{0max} from M_{0true} for all B hadrons. Although approximately 20% of the B hadrons are B_s^0 and Λ_b which have larger masses, the values of M_{0max} obtained using $M_B=5.28 \text{ GeV}/c^2$ in Equation (6) are typically within about 10% of M_0 . The distribution of the reconstructed M_{0max}^2 for vertices in the selected B hadron sample is shown in Figure 3. The simulation indicates that the non- $b\bar{b}$ background is concentrated at high M_{0max}^2 ; this because most of the light flavor vertices have small M_{Pt} and therefore, due to the strong negative correlation between M_{Pt} and M_{0max} , large M_{0max} . The negative tail in Figure 3 is an effect of detector resolution, and the Monte Carlo simulation shows good agreement with the data.

Because M_0 peaks near M_{0max} , we set $M_0^2 = M_{0max}^2$ if $M_{0max}^2 \geq 0$, and $M_0^2 = 0$ if $M_{0max}^2 < 0$. We then calculate P_{0l} :

$$P_{0l} = \frac{M_B^2 - (M_{ch}^2 + P_t^2) - (M_0^2 + P_t^2)}{2(M_{ch}^2 + P_t^2)} P_{chl}, \quad (7)$$

and hence E_0 (Equation (3)). We then divide the reconstructed B hadron energy, $E_B^{rec} = E_0 + E_{ch}$, by the beam energy, $E_{beam} = \sqrt{s}/2$, to obtain the reconstructed scaled B hadron energy, $x_B^{rec} = E_B^{rec}/E_{beam}$.

The resolution of x_B^{rec} depends on both M_{0max}^2 and the true x_B , x_B^{true} . Vertices in the negative tail of the M_{0max}^2 distribution that have $M_{0max}^2 < -1.0(\text{GeV}/c^2)^2$ are often poorly reconstructed and are not used in further analysis. Vertices with small values of $|M_{0max}^2|$ are typically reconstructed with better resolution and an upper cut on M_{0max}^2

is hence applied. For an x_B -independent cut, the efficiency for selecting B hadrons is roughly linear in x_B^{true} . In order to obtain an approximately x_B -independent selection efficiency we choose the following upper cut:

$$M_{0max}^2 < \{1.1 + 0.007(E_{beam} - E_B^{rec}) + 4.0exp[-(E_B^{rec} - 5.5)/3.5]\}^2, \quad (8)$$

where the two terms that depend on the reconstructed energy E_B^{rec} increase the efficiency at lower B hadron energy.

Only about 0.6% of the selected vertices are from light-flavor events, but they are concentrated in the lowest energy bin. To further remove this background, a vertex is required to contain at least 3 quality tracks with a normalized impact parameter greater than 2. This eliminates about 36% (30%) of the uds (charm) background overall and 78% (44%) in the few lowest energy bins. This cut helps to reduce the dependence of the reconstructed B hadron energy distribution on the light flavor simulation in the low energy region, which is a good step towards finding the correct shape of the B hadron energy distribution at low energies. Figure 4 shows the distribution of M_{0max}^2 after all these cuts; the data and Monte Carlo simulation are in good agreement.

A total of 4,164 vertices in the data for 1997-98 satisfy all these selection cuts. The overall efficiency for selecting B hadrons is 4.17% and the estimated B hadron purity is 99.0% with a uds (charm) background of 0.4% (0.6%). The efficiency as a function of x_B^{true} is shown in Figure 5. The dependence is rather weak except for the lowest x_B region; the efficiency is substantial, about 2.0% even just above the kinematic threshold for B energy.

We examine the B -energy resolution of this technique. The distribution of the normalized difference between the true and reconstructed B hadron energies, $(x_B^{rec} - x_B^{true})/x_B^{true}$, for Monte Carlo events is fitted with a sum of two Gaussians. A feature of the analysis is that the distribution is symmetric and the fitted mean values are generally consistent with zero. The fit yields a core width (the width of the narrower Gaussian) of 9.6% and a tail width (the width of the wider Gaussian) of 21.2% with a core fraction of 83.6%. Figure 6 shows the core and tail widths as a function of x_B^{true} . In order to compare the widths from different x_B bins, we fix the ratio between core and tail fractions to that obtained in the overall fit above. The x_B -dependence of the resolution is weak, indicating that the absolute resolution on x_B , $x_B^{rec} - x_B^{true}$, is very good at low B energy, which is an advantage of this energy reconstruction technique.

Figure 7 shows the distribution of the reconstructed scaled B hadron energy for the data, $D^{data}(x_B^{rec})$, and for the Monte Carlo simulation, $D^{MC}(x_B^{rec})$. The small non- $b\bar{b}$ background, the high B selection efficiency over the full kinematic coverage, and the good energy resolution combine to give a much improved sensitivity of the data to the underlying true *shape* of the B energy distribution (see next section).

The event generator used in our simulation is based on a perturbative QCD ‘parton shower’ for production of quarks and gluons, together with the phenomenological Peterson function [7] (Table 4.1) to account for the fragmentation of b and c quarks into B and D hadrons, respectively, within the iterative Lund string hadronisation mecha-

nism [23]; this simulation yields a ‘generator-level’ primary B hadron energy distribution with $\langle x_B \rangle = 0.693^*$. It is apparent that this simulation does not reproduce the data well (Figure 7); the χ^2 for the comparison is 70.3 for 16 bins[†].

The distribution of the non- $b\bar{b}$ background, $S(x_B^{rec})$, is also shown in Figure 7. The background is subtracted bin-by-bin from the $D^{data}(x_B^{rec})$ before we proceed to test various fragmentation models.

4 The Shape of the B Hadron Energy Distribution

Given the raw reconstructed B energy distribution in the data shown in Figure 7, there are several ways of estimating the true underlying B energy distribution. Here we take two approaches, each described in a subsection.

In the first part, we test several b fragmentation models, $f(z, \beta)$ embedded within Monte Carlo generators, where z is an internal, experimentally inaccessible variable, corresponding roughly to the fraction of the momentum of the fragmenting b quark carried by the resulting B hadron, and β is the set of parameters associated with the model in question. In the second part, we test several functional forms for the distribution of x_B itself, $f(x_B, \lambda)$, where λ represents the set of parameters associated with each functional form.

4.1 Tests of b Quark Fragmentation Models $f(z, \beta)$

We first consider testing models of b quark fragmentation. Since the fragmentation functions for various models are usually functions of an experimentally inaccessible variable (e.g. $z = (E + p_{\parallel})_H / (E + p_{\parallel})_Q$ or $z = p_{\parallel H} / p_{\parallel Q}$), it is necessary to use a Monte Carlo generator to generate events according to a given input heavy quark fragmentation function $f(z, \beta)$, where β represents the set of parameters.

We consider the phenomenological models of the Lund group [5], Bowler [6], Peterson *et al.* [7] and Kartvelishvili *et al.* [30]. We also consider the perturbative QCD calculations of Braaten *et al.* (BCFY) [4], and of Collins and Spiller (CS) [31]. We use the JETSET [23] parton shower Monte Carlo and each fragmentation model in question to generate the simulated events without detector simulation. Table 4.1 contains a list of the models. In addition, we test the UCLA [33] fragmentation model with default parameters, as there is no explicit parameter controlling the B hadron energy. For b fragmentation, we also test the HERWIG [32] event-generator using both possible values of the parameter $clidir = 0$ and 1.

In order to make a consistent comparison of each model with the data we adopt the following procedure. For each model, starting values of the arbitrary parameters, β , are assigned and the corresponding fragmentation function $f(z, \beta)$ is used along with the

*We used a value of the Peterson function parameter $\epsilon_b = 0.006$ [29].

†We exclude several bins with very few events in the comparison. For details see Section 4.1.

Model	$f(z, \beta)$	Reference
BCFY	$\frac{z(1-z)^2}{[1-(1-r)z]^6} [3 + \sum_{i=1}^4 (-z)^i f_i(r)]$	[4]
Bowler	$\frac{1}{z^{(1+r_b m_\perp^2)}} (1-z)^a \exp(-b m_\perp^2 / z)$	[6]
CS	$(\frac{1-z}{z} + \frac{(2-z)\epsilon_b}{1-z})(1+z^2)(1-\frac{1}{z} - \frac{\epsilon_b}{1-z})^{-2}$	[31]
Kartvelishvili	$z^{\alpha_b}(1-z)$	[30]
Lund	$\frac{1}{z}(1-z)^a \exp(-b m_\perp^2 / z)$	[5]
Peterson	$\frac{1}{z}(1-\frac{1}{z} - \frac{\epsilon_b}{1-z})^{-2}$	[7]

Table 1: b quark fragmentation models used in comparison with the data. For the BCFY model, $f_1(r) = 3(3-4r)$, $f_2(r) = 12-23r+26r^2$, $f_3(r) = (1-r)(9-11r+12r^2)$, and $f_4(r) = 3(1-r)^2(1-r+r^2)$.

JETSET Monte Carlo to produce the corresponding scaled primary B hadron energy distribution, $D^{MC}(x_B^{true})$ in the MC-generated $b\bar{b}$ event sample, *before* simulation of the detector. Then each simulated B hadron is weighted according to its true B hadron energy, x_B^{true} ; the weight is determined by the ratio of the generated B hadron energy distribution, $D^{MC}(x_B^{true})$, to that of our default simulation $D^{default}(x_B^{true})$. After simulation of the detector, application of the analysis cuts and background subtraction, the resulting weighted distribution of reconstructed B hadron energies, $D^{MC}(x_B^{rec})$, is then compared with the background-subtracted data distribution and the χ^2 value, defined as

$$\chi^2 = \sum_{i=1}^N \left(\frac{N_i^{data} - r N_i^{MC}}{\sigma_i} \right)^2 \quad (9)$$

is calculated, where N is the number of bins to be used in the comparison, N_i^{data} is the number of entries in bin i in the data distribution, and N_i^{MC} is the number of entries in bin i in the simulated distribution[‡]. σ_i is the statistical error on the deviation of the observed number of entries for the data from the expected number of entries in bin i , which can be expressed as

$$\sigma_i^2 = \left(\sqrt{r N_i^{MC}} \right)^2 + \left(r \sqrt{N_i^{MC}} \right)^2, \quad (10)$$

where $\left(\sqrt{r N_i^{MC}} \right)^2$ is the expected statistical variance on the observed data number of entries in bin i , assuming the model being tested is correct, and $\left(r \sqrt{N_i^{MC}} \right)^2$ is the statistical variance on the expected number of entries in bin i . Since the χ^2 -test is not

[‡] r is the factor by which the total number of entries in the simulated distribution is scaled to the number of entries in the data distribution; $r \simeq 1/12$.

a statistically effective test for bins with a very small number of entries, the third, the fourth, and the last three bins in Figure 7 are excluded from the comparison.

We vary the values of the set of parameters β and repeat the above procedure. The minimum χ^2 is found by scanning through the input parameter space, yielding a set of parameters which give an optimal description of the reconstructed data by the fragmentation model in question. Each of the nine plots in Figure 8 shows the background-subtracted distribution of reconstructed B hadron energy for the data (points) and the respective B energy distribution (histogram) resulting *either* from the optimised input fragmentation function $f(z)$ embedded within the JETSET parton shower simulation, *or* from the predictions of the HERWIG event-generator and the UCLA fragmentation model. Data points excluded from the fit are represented in Figure 8 by open circles. Table 4.1 lists the results of the comparisons.

Model	χ^2/dof	Parameters	$\langle x_B \rangle$
JETSET + BCFY	105/16	$r = 0.085$	0.694
JETSET + Bowler*	17/15	$a = 1.4, b = 1.2, (r_b = 1)$	0.709
JETSET + Collins and Spiller	142/16	$\epsilon_b = 0.003$	0.691
JETSET + Kartvelishvili* <i>et al.</i>	32/16	$\alpha_b = 10.0$	0.708
JETSET + Lund*	17/15	$a = 1.4, b = 0.4$	0.712
JETSET + Peterson <i>et al.</i>	70/16	$\epsilon_b = 0.0055$	0.700
HERWIG cldir=0	1015/17	—	0.632
HERWIG cldir=1	149/17	—	0.676
UCLA*	27/17	—	0.718

Table 2: Results of fragmentation model tests for JETSET + fragmentation models, the HERWIG model and the UCLA model. Minimum χ^2 , number of degrees of freedom, corresponding parameter values, and the mean value of the corresponding B energy distribution are listed. A * indicates the models used below to correct the data.

We conclude that with our resolution and our current data sample, we are able to distinguish between several fragmentation models. Within the context of the JETSET Monte Carlo, the Lund and Bowler models are consistent with the data with χ^2 probabilities of 31% and 35%, respectively, the Kartvelishvili model is consistent with the data at the 1% level, while the Peterson, the BCFY and the CS models are found to be inconsistent with the data. The UCLA model is consistent with the data to a level of 6% χ^2 probability. The HERWIG model with $cldir = 0$ is confirmed to be much too soft. Using $cldir = 1$ results in a substantial improvement, but it is still inconsistent with the data.

4.2 Tests of Functional Forms $f(x_B, \lambda)$

We then consider the more general question of what functional forms of the B energy distribution, $f(x_B, \lambda)$, can be used as estimates of the true underlying B energy distribution. In particular, we would like to test a wide variety of functional forms and ask how many different forms are consistent with the data. Each consistent functional form will add to the list of our estimates of the true underlying B energy distribution.

For convenience we consider the functional forms of the BCFY, Collins and Spiller, Kartvelishvili, Lund, and Peterson groups in the variable x_B . In addition we consider *ad hoc* generalisations of the Peterson function (F), an 8th-order polynomial and a ‘power’ function. These functions are listed in Table 3. Each function vanishes at $x_B = 0$ and $x_B = 1$.

Function	$f(x_B, \lambda)$	Reference
F	$\frac{(1 + b(1 - x_B))}{x_B} \left(1 - \frac{c}{x_B} - \frac{d}{1 - x_B}\right)^{-2}$	[13]
8th-order Polynomial	$x_B(1 - x_B)(x_B - x_B^0)(1 + \sum_{i=1}^5 p_i x_B^i)$	(see text)
Power	$x_B^\alpha(1 - x_B)^\beta$	(see text)

Table 3: B energy functional forms used in comparison with the data. A polynomial function and a power function are included (see text for discussion). x_B^0 is the low kinematic threshold for B energy.

For each functional form, a testing procedure similar to that described in subsection 4.1 is applied. The optimised fitting parameters λ and the minimum χ^2 values are listed in Table 4.2. The corresponding $D^{MC}(x_B^{rec})$ are compared with the data in Figure 9.

Two sets of optimised parameters are found for the generalised Peterson function F to describe the data. ‘F1’, obtained by setting the parameter b (shown in Table 3) to infinity, behaves like x_B as $x_B \rightarrow 0$ and $(1 - x_B)^3$ as $x_B \rightarrow 1$ and yields a χ^2 probability of 18%; ‘F2’, obtained by setting b to zero, has a χ^2 probability of 1.0%. A constrained polynomial of at least 8th-order is needed to obtain a χ^2 probability greater than 0.1%. The Peterson functional form marginally reproduces the data with a χ^2 probability of about 1%. The remaining functional forms are found to be inconsistent with our data. The widths of the BCFY and CS functions are too large to describe the data; Kartvelishvili, Lund and the ‘power’ functional form vanish too fast as x_B approaches zero. We conclude that, within our resolution and with our current data sample, we are able to distinguish between some of these functional forms. But most importantly, consistent functional forms will help us evaluate the uncertainty on the true B energy distribution.

Function	χ^2/dof	Parameters	$\langle x_B \rangle$
F1*	20/15	$c = 0.884 \pm 0.014$ $d = 0.0181 \pm 0.0015$	0.707±0.003
F2*	31/15	$c = 0.976 \pm 0.029$ $d = 0.039 \pm 0.002$	0.710±0.003
BCFY	73/16	$r = 0.248 \pm 0.007$	0.704±0.003
Collins and Spiller	75/16	$\epsilon_b = 0.0519 \pm 0.0036$	0.706±0.003
Kartvelishvili <i>et al.</i>	138/16	$\alpha_b = 3.904 \pm 0.072$	0.710±0.003
Lund	252/15	$a = 1.88 \pm 0.08$ $bm_{\perp}^2 = 0.32 \pm 0.05$	0.715±0.003
Peterson <i>et al.</i> *	31/16	$\epsilon_b = 0.0382 \pm 0.0016$	0.709±0.003
Polynomial*	12/12	$p_1 = -9.99 \pm 0.25$ $p_2 = 40.84 \pm 0.25$ $p_3 = -82.26 \pm 0.68$ $p_4 = 80.90 \pm 0.76$ $p_5 = -30.60 \pm 0.54$	0.709±0.003
Power	133/15	$\alpha = 3.73 \pm 0.17$ $\beta = 0.84 \pm 0.07$	0.713±0.003

Table 4: Results of the χ^2 fit of fragmentation functions to the reconstructed B hadron energy distribution after background subtraction. The minimum χ^2 value, the number of degrees of freedom, the corresponding parameter values, and the mean value of the corresponding B energy distribution are listed. Errors are statistical only. A * indicates those forms used below to correct the data.

5 Correction of the B Energy Distribution

In order to compare our results with those from other experiments and potential future theoretical predictions it is necessary to correct the reconstructed scaled B hadron energy distribution $D^{data}(x_B^{rec})$ for the effects of non- B backgrounds, detector acceptance, event selection and analysis bias, and initial-state radiation, as well as for bin-to-bin migration effects caused by the finite resolution of the detector and the analysis technique. Due to the known rapid variation of the yet-unknown true B energy distribution at large x_B , *any* correction procedure will necessarily be more or less model-dependent. We choose a method that explicitly evaluates this model-dependence and gives a very good estimate of the true energy distribution using all of the above models or functional forms that are at least marginally consistent with the data.

We apply a 25×25 matrix unfolding procedure to $D^{data}(x_B^{rec})$ to obtain an estimate of the true distribution $D^{data}(x_B^{true})$:

$$D^{data}(x_B^{true}) = \epsilon^{-1}(x_B^{true}) \cdot E(x_B^{true}, x_B^{rec}) \cdot (D^{data}(x_B^{rec}) - S(x_B^{rec})) \quad (11)$$

where S is a vector representing the background contribution, E is a matrix to correct for bin-to-bin migrations, and ϵ is a vector representing the efficiency for selecting true B hadron decays for the analysis. The matrices S , E and ϵ are calculated from our MC simulation; the matrix E incorporates a convolution of the input fragmentation function with the resolution of the detector. $E(i, j)$ is the number of vertices with x_B^{true} in bin i and x_B^{rec} in bin j , normalized by the total number of vertices with x_B^{rec} in bin j .

We evaluate the matrix E using the Monte Carlo simulation weighted according to an input generator-level *true* B energy distribution found to be consistent with the data in Section 4. We have seen that several B energy distributions can reproduce the data. We consider in turn each of these eight consistent distributions, using the optimised parameters listed in Table 4.1 and 4.2. The matrix E is then evaluated by examining the population migrations of true B hadrons between bins of the input scaled B energy, x_B^{true} , and the reconstructed scaled B energy, x_B^{rec} . Using each $D^{MC}(x_B^{true})$, the data distribution $D^{data}(x_B^{rec})$ is then unfolded according to Equation (11) to yield $D^{data}(x_B^{true})$, which is shown for each input fragmentation function in Figure 10.

It can be seen that the shapes of $D^{data}(x_B^{true})$ differ systematically among the input b quark fragmentation models and the assumed B energy functional forms. These differences are used to assign systematic errors. Figure 11 shows the final corrected x_B distribution $D(x_B)$, which is the bin-by-bin average of the eight unfolded distributions, where the inner error bar represents the statistical error and the outer error bar is the sum in quadrature of the r.m.s. of the eight unfolded distributions and the statistical error within each bin. Since two of the eight functions (the Kartvelishvili model and the Peterson functional form) are only in marginal agreement with the data, and the 8th-order polynomial has a slightly unphysical behavior near $x_B = 1$, this r.m.s. may be considered to be a rather reasonable envelope within which the true x_B distribution is most likely to vary. The model dependence for this analysis is significantly smaller than those of previous direct B energy measurements, indicating the enhanced sensitivity of our data to the underlying true energy distribution.

6 Systematic Errors

We have considered sources of systematic uncertainty that potentially affect our measurement of the B hadron energy distribution. These may be divided into uncertainties in modelling the detector and uncertainties on experimental measurements serving as input parameters to the underlying physics modelling. For these studies our standard simulation, employing the Peterson fragmentation function, is used.

For each source of systematic error, the Monte Carlo distribution $D^{MC}(x_B^{true})$ is re-weighted and then the resulting Monte Carlo reconstructed distribution $D^{MC}(x_B^{rec})$ is compared with the data $D^{data}(x_B^{rec})$ by repeating the fitting and unfolding procedures described in Section 4 and 5. The differences in both the shape and the mean value of the x_B^{true} distribution relative to the standard procedure with nominal values of parameters are considered. Due to the strong dependence of our energy reconstruction

technique on charged tracks, the dominant systematic error is due to the discrepancy in the charged track transverse momentum resolution between the Monte Carlo and the data. We evaluate this conservatively by taking the full difference between the nominal results and results using a resolution-corrected Monte Carlo event sample. The difference between the measured and simulated charged track multiplicity as a function of $\cos\theta$ and momentum is attributed to an unsimulated tracking inefficiency correction. We use a random track-tossing procedure to evaluate the difference in our results.

Source	Variation	$\delta \langle x_B \rangle$
Monte Carlo statistics		0.0008
Tracking efficiency correction	on/off	0.0022
Track impact parameter	on/off	0.0012
Track polar angle	2 mrad	-0.0009
Track $1/P_\perp$	0.0008	-0.0025
Hadronic event selection	standard	0.0005
Total Detector Systematics		0.0037
B^0 mass effect	$\pm 2\sigma$	0.0001
B lifetimes	$\pm\sigma$	0.0002
$B^+/B^0/B_s^0/\Lambda_b$ production	$\pm 2\sigma$	0.0010
B decay fraction	$\pm 2\sigma$	0.0006
B decay $\langle n_{ch} \rangle$	5.3 ± 0.3	0.0012
D lifetimes	$\pm\sigma$	0.0002
D decay $\langle n_{ch} \rangle$	$\pm\sigma$	0.0005
$D \rightarrow K^0$ multiplicity	$\pm\sigma$	0.0013
$D \rightarrow \text{no } \pi^0$ fraction	$\pm\sigma$	0.0005
$g \rightarrow b\bar{b}$	$(0.31 \pm 0.15)\%$	0.0002
$g \rightarrow c\bar{c}$	$(2.4 \pm 1.2)\%$	0.0008
K^0 production	0.66 ± 0.07 trks	0.0009
Λ production	0.12 ± 0.01 trks	0.0002
R_b	0.2170 ± 0.0009	< 0.0001
R_c	0.1733 ± 0.0048	< 0.0001
Total Systematics		0.0047

Table 5: Source and systematic errors.

A large number of measured quantities relating to the production and decay of charm and bottom hadrons are used as input to our simulation. In $b\bar{b}$ events we have considered the uncertainties on: the branching fraction for $Z^0 \rightarrow b\bar{b}$; the rates of production of B^\pm , B^0 and B_s^0 mesons, and B baryons; the lifetimes of B mesons and baryons; and the average B hadron decay charged multiplicity. In $c\bar{c}$ events we have considered the uncertainties on: the branching fraction for $Z^0 \rightarrow c\bar{c}$; the charmed hadron lifetimes,

the charged multiplicity of charmed hadron decays, the production of K^0 from charmed hadron decays, and the fraction of charmed hadron decays containing no π^0 s. We have also considered the rate of production of $s\bar{s}$ in the jet fragmentation process, and the production of secondary $b\bar{b}$ and $c\bar{c}$ from gluon splitting. The world-average values [10, 29] of these quantities used in our simulation, as well as the respective uncertainties, are listed in Table 6. Most of these variations have effect on normalisation, but very little on the shape or the mean value. In no case do we find a variation that changes our conclusion about which functions are consistent with the data. Systematic errors on the mean value are listed in Table 6.

The model-dependence of the unfolding procedure is estimated by considering the envelope of the unfolded results illustrated in Figure 11. Since eight functions provide an acceptable χ^2 probability in fitting to the data, in each bin of x_B we calculated the average value of these eight unfolded results as well as the r.m.s. deviation. In each bin the average value is taken as our central value and the r.m.s. value is assigned as the unfolding uncertainty.

Other relevant systematic effects such as variation of the event selection cuts and the assumed B hadron mass are also found to be very small. As a cross-check, we vary the M_{0max} cut (Equation (8)) in selecting the final B sample within a large range and repeat the analysis procedure. In each case, conclusions about the shape of the B energy distribution hold. In each bin, all sources of systematic uncertainty are added in quadrature to obtain the total systematic error.

7 Measurement of $B - \bar{B}$ Energy Correlations

We next considered events in which we found secondary vertices corresponding to both the leading B and \bar{B} hadrons. In order to maximize our efficiency for finding both vertices, and eliminate events in which we found two vertices from the same B/\bar{B} hadron, we followed the selection procedure described in Section 3 with the following modifications: 1) The Durham algorithm was applied to selected hadronic events, with a y_c parameter value of 0.015, in order to define a jet structure in each event. 2) Events were retained in which a secondary vertex was found in exactly two of the reconstructed jets, labelled arbitrarily 1 and 2, and in which: both vertices satisfied $-1 < M_{0max}^2 < 12$ $(\text{GeV}/c^2)^2$, both vertices had a distance from the IP of at least 1 mm, at least one vertex contained at least two tracks with a normalised impact-parameter significance of at least 2σ w.r.t. the IP, at least one vertex satisfied $M_{Pt} > 2 \text{ GeV}/c^2$, both reconstructed B energies satisfied $0 < E_B^{rec} < 60 \text{ GeV}$, and the angle (ϕ) between the vertex axes of jets 1 and 2 satisfied $\cos\phi < 0.99$. A sample of 17707 events was selected, estimated to be 99.9% pure in $Z^0 \rightarrow b\bar{b}$ events, and the efficiency for selecting a true $b\bar{b}$ event was estimated to be 32%.

We quantified the correlation between the two B hadrons in terms of the moments proposed in [16]. We first evaluated the moments of the one dimensional $D(x_B)$ from the raw measured distribution. The procedure was the same as described in Section 3,

except that instead of Eq. 8 we imposed the requirement:

$$M_{0max}^2 < 15(GeV^2/c^4).$$

The moments

$$D_i^{rec} \equiv \int (x_B^{rec})^i dN/dx_B^{rec} dx_B^{rec},$$

were evaluated, from which we calculated the factors M_i^{rec} , where

$$D_i^{rec} = M_i^{rec} P_i$$

and the P_i were evaluated at leading order in pQCD and are tabulated in [16].

We then evaluated the double moments of the correlated B energy distribution $d^2N/dx_{B1}dx_{B2}$.

Using this sample we formed the correlated B -energy distribution $d^2N/(dx_{B1}^{rec}dx_{B2}^{rec})$ and evaluated the double moments:

$$D_{ij}^{rec}(\phi) \equiv \int \int (x_{B1}^{rec})^i (x_{B2}^{rec})^j d^2N(\phi)/(dx_{B1}^{rec}dx_{B2}^{rec}) dx_{B1}^{rec}dx_{B2}^{rec},$$

where x_{B1}^{rec} and x_{B2}^{rec} are the reconstructed scaled energies of the two B hadrons. We then formed the quantities:

$$P_{ij}^{rec}(\phi) = D_{ij}^{rec}(\phi)/(M_i^{rec} M_j^{rec})$$

and corrected them for detector effects using a standard bin-by-bin method. The corrected, normalized quantities $P_{ij}(\phi)/P_{11}(\phi)$ are shown in Fig. 12. A LO pQCD calculation [16] of the corresponding normalised double moments is also shown in Fig. 12; the calculation reproduces the data, which verifies the ansatz of factorisation used in this calculation of b fragmentation.

8 Summary and Conclusions

We have used the excellent tracking and vertexing capabilities of SLD to reconstruct the energies of B hadrons in $e^+e^- \rightarrow Z^0$ events over the full kinematic range by applying a new kinematic technique to an *inclusive* sample of topologically reconstructed B hadron decay vertices. The overall B selection efficiency of the method is 3.9%. We estimate the resolution on the B energy to be about 10.4% for roughly 83% of the reconstructed decays. The energy resolution for low energy B hadrons is significantly better than previous measurements.

In order to get a good estimate of the model dependence of the unfolded distribution, the distribution of reconstructed scaled B hadron energy, $D^{data}(x_B^{rec})$, is compared **case 1)** with predictions of *either* perturbative QCD and phenomenological b quark fragmentation models in the context of the JETSET parton shower Monte Carlo, *or* HERWIG and UCLA fragmentation models, and **case 2)** with a set of functional forms for the B

energy distribution. In **case 1**), the Lund and the Bowler models are consistent with the data; the model of Kartvelishvili *et al.* is in marginal agreement with the data. The models based on the perturbative QCD calculations of Braaten *et al.*, and of Collins and Spiller, and the Peterson model are disfavored by the data. Although both versions of the HERWIG model are excluded by the data, the new version is very much improved. The UCLA model describes the data reasonably well. In **case 2**), four functional forms, namely the two generalised Peterson functions F1 and F2, the Peterson function, and a constrained 8th-order polynomial are found to be consistent with the data.

The raw B energy distribution is then corrected for bin-to-bin migrations caused by the resolution of the method and for selection efficiency to derive the energy distribution of the weakly decaying B hadrons produced in Z^0 decays. Systematic uncertainties in the correction have been evaluated and are found to be significantly smaller than those of previous direct B energy measurements. The final corrected x_B distribution $D^{data}(x_B^{true})$ is shown in Figure 11. The statistical and unfolding uncertainties are indicated separately.

It is conventional to evaluate the mean of this B energy distribution, $\langle x_B \rangle$. For each of the eight functions providing a reasonable description of the data (four from **case 1**) and four from **case 2**)), we evaluate $\langle x_B \rangle$ from the distribution that corresponds to the optimised parameters; these are listed in Table 4.1 and Table 4.2. We take the average of the eight values of $\langle x_B \rangle$ as our central value, and define the model-dependent uncertainty to be the r.m.s. deviation within each bin. All detector and physics modeling systematic errors are included. We obtain

$$\langle x_B \rangle = 0.710 \pm 0.003(stat.) \pm 0.005(syst) \pm 0.004(model), \quad (12)$$

It can be seen that $\langle x_B \rangle$ is relatively insensitive to the variety of allowed forms of the shape of the fragmentation function $D(x_B)$.

Finally, we have made the first measurement of the correlated B -energy distribution. From comparison of the double moments of this distribution with the moments of $D(x_B)$ we find that a leading-order pQCD calculation reproduces the data, which verifies the ansatz of factorisation employed in the pQCD calculation.

Acknowledgements

We thank the personnel of the SLAC accelerator department and the technical staffs of our collaborating institutions for their outstanding efforts on our behalf.

*Work supported by Department of Energy contracts:

DE-FG02-91ER40676 (BU), DE-FG03-91ER40618 (UCSB), DE-FG03-92ER40689 (UCSC),
DE-FG03-93ER40788 (CSU), DE-FG02-91ER40672 (Colorado), DE-FG02-91ER40677 (Illinois),
DE-AC03-76SF00098 (LBL), DE-FG02-92ER40715 (Massachusetts), DE-FC02-94ER40818 (MIT),
DE-FG03-96ER40969 (Oregon), DE-AC03-76SF00515 (SLAC), DE-FG05-91ER40627 (Tennessee),
DE-FG02-95ER40896 (Wisconsin), DE-FG02-92ER40704 (Yale);

National Science Foundation grants:

PHY-91-13428 (UCSC), PHY-89-21320 (Columbia), PHY-92-04239 (Cincinnati),
PHY-95-10439 (Rutgers), PHY-88-19316 (Vanderbilt), PHY-92-03212 (Washington);
The UK Particle Physics and Astronomy Research Council (Brunel, Oxford and RAL);
The Istituto Nazionale di Fisica Nucleare of Italy
(Bologna, Ferrara, Frascati, Pisa, Padova, Perugia);
The Japan-US Cooperative Research Project on High Energy Physics (Nagoya, Tohoku);
The Korea Research Foundation (Soongsil, 1997).

References

- [1] See e.g. J.D. Bjorken, Phys. Rev. **D17** (1978) 171.
- [2] B. Mele and P. Nason, Phys. Lett. **B245** (1990) 635.
B. Mele and P. Nason, Nucl. Phys. **B361** (1991) 626.
G. Colangelo and P. Nason, Phys. Lett. **B285** (1992) 167.
- [3] Yu. L. Dokshitzer, V.A. Khoze, S.I. Troyan, Phys. Rev. **D53** (1996) 89.
- [4] E. Braaten, K. Cheung, T.C. Yuan, Phys. Rev. **D48** (1993) R5049.
E. Braaten, K. Cheung, S. Fleming, T.C. Yuan, Phys. Rev. **D51** (1995) 4819.
- [5] B. Andersson, G. Gustafson, G. Ingelman, T. Sjöstrand, Phys. Rep. **97** (1983) 32.
- [6] M.G. Bowler, Z. Phys. **C11** (1981) 169.
- [7] C. Peterson, D. Schlatter, I. Schmitt and P.M. Zerwas, Phys. Rev. **D27** (1983) 105.
- [8] R.L.Jaffe, L.Randall, Nucl. Phys. **B412** (1994) 79.
- [9] L. Randall, N. Rius, Nucl. Phys. **B441** (1995) 167.
- [10] The LEP Electroweak Working Group, D. Abbaneo *et al.*, LEPHF/96-01 (July 1996).
- [11] ALEPH Collab., D. Buskulic *et al.*, Z. Phys. **C62** (1994) 179.
DELPHI Collab., P. Abreu *et al.*, Z. Phys. **C66** (1995) 323.
L3 Collab., O. Adeva *et al.*, Phys Lett. **B261** (1991) 177.
OPAL Collab., P.D. Acton *et al.*, Z. Phys. **C60** (1993) 199.
- [12] See e.g. D.H. Saxon in 'High Energy Electron-Positron Physics', Eds. A. Ali, P. Söding,
World Scientific 1988, p. 539.
- [13] ALEPH Collab., D. Buskulic *et al.*, Phys. Lett. **B357** (1995) 699.
- [14] OPAL Collab., G. Alexander *et al.*, Phys. Lett. **B364** (1995) 93.

- [15] SLD Collab., K. Abe *et al.*, Phys. Rev. **D56** (1997) 5310.
- [16] P.N. Burrows, P. Hoyer, V. Del Duca, Z. Phys. **C53** (1992) 149.
- [17] SLD Design Report, SLAC Report 273 (1984).
- [18] SLD Collaboration, K. Abe *et al.*, Phys. Rev. **D51** (1995) 962.
- [19] M.D. Hildreth *et al.*, IEEE Trans. Nucl. Sci. **42** (1994) 451.
- [20] C.J.S. Damerell *et al.*, Nucl. Instr. Meth. **A400** (1997) 287.
- [21] S. Brandt *et al.*, Phys. Lett. **12** (1964) 57.
E. Farhi, Phys. Rev. Lett. **39** (1977) 1587.
- [22] D. Axen *et al.*, Nucl. Inst. Meth. **A328** (1993) 472.
- [23] T. Sjöstrand, Comput. Phys. Commun. **82** (1994) 74.
- [24] P. N. Burrows, Z. Phys. **C41** (1988) 375.
OPAL Collab., M.Z. Akrawy *et al.*, Z. Phys. **C47** (1990) 505.
- [25] SLD Collab., K. Abe *et al.*, SLAC-PUB-7117; to appear in Phys. Rev. Lett.
- [26] R. Brun *et al.*, Report No. CERN-DD/EE/84-1 (1989).
- [27] D. J. Jackson, Nucl. Inst. and Meth. **A388**, 247 (1997).
- [28] SLD Collab., K. Abe *et al.*, Phys. Rev. Lett. **80** (1998) 660.
- [29] SLD Collab., K. Abe *et al.*, Phys. Rev. **D53** (1996) 1023.
- [30] V. G. Kartvelishvili, A. K. Likhoded and V. A. Petrov, Phys. Lett. **78B** (1978) 615.
- [31] P.D.B. Collins and T.P. Spiller, J. Phys. G **11** (1985) 1289.
- [32] G. Marchesini *et al.*, Comp. Phys. Comm. **67** (1992) 465.
- [33] S. Chun and C. Buchanan, Phys. Rep. **292** (1998) 239.

**List of Authors

Koya Abe,⁽²⁴⁾ Kenji Abe,⁽¹⁵⁾ T. Abe,⁽²¹⁾ I. Adam,⁽²¹⁾ H. Akimoto,⁽²¹⁾ D. Aston,⁽²¹⁾
 K.G. Baird,⁽¹¹⁾ C. Baltay,⁽³⁰⁾ H.R. Band,⁽²⁹⁾ T.L. Barklow,⁽²¹⁾ J.M. Bauer,⁽¹²⁾ G. Bellodi,⁽¹⁷⁾
 R. Berger,⁽²¹⁾ G. Blaylock,⁽¹¹⁾ J.R. Bogart,⁽²¹⁾ G.R. Bower,⁽²¹⁾ J.E. Brau,⁽¹⁶⁾
 M. Breidenbach,⁽²¹⁾ W.M. Bugg,⁽²³⁾ D. Burke,⁽²¹⁾ T.H. Burnett,⁽²⁸⁾ P.N. Burrows,⁽¹⁷⁾
 A. Calcaterra,⁽⁸⁾ R. Cassell,⁽²¹⁾ A. Chou,⁽²¹⁾ H.O. Cohn,⁽²³⁾ J.A. Coller,⁽⁴⁾ M.R. Convery,⁽²¹⁾
 V. Cook,⁽²⁸⁾ R.F. Cowan,⁽¹³⁾ G. Crawford,⁽²¹⁾ C.J.S. Damerell,⁽¹⁹⁾ M. Daoudi,⁽²¹⁾
 N. de Groot,⁽²⁾ R. de Sangro,⁽⁸⁾ D.N. Dong,⁽¹³⁾ M. Doser,⁽²¹⁾ R. Dubois, I. Erofeeva,⁽¹⁴⁾
 V. Eschenburg,⁽¹²⁾ E. Etzion,⁽²⁹⁾ S. Fahey,⁽⁵⁾ D. Falciari,⁽⁸⁾ J.P. Fernandez,⁽²⁶⁾ K. Flood,⁽¹¹⁾
 R. Frey,⁽¹⁶⁾ E.L. Hart,⁽²³⁾ K. Hasuko,⁽²⁴⁾ S.S. Hertzbach,⁽¹¹⁾ M.E. Huffer,⁽²¹⁾ X. Huynh,⁽²¹⁾
 M. Iwasaki,⁽¹⁶⁾ D.J. Jackson,⁽¹⁹⁾ P. Jacques,⁽²⁰⁾ J.A. Jaros,⁽²¹⁾ Z.Y. Jiang,⁽²¹⁾
 A.S. Johnson,⁽²¹⁾ J.R. Johnson,⁽²⁹⁾ R. Kajikawa,⁽¹⁵⁾ M. Kalelkar,⁽²⁰⁾ H.J. Kang,⁽²⁰⁾
 R.R. Kofler,⁽¹¹⁾ R.S. Kroeger,⁽¹²⁾ M. Langston,⁽¹⁶⁾ D.W.G. Leith,⁽²¹⁾ V. Lia,⁽¹³⁾ C. Lin,⁽¹¹⁾
 G. Mancinelli,⁽²⁰⁾ S. Manly,⁽³⁰⁾ G. Mantovani,⁽¹⁸⁾ T.W. Markiewicz,⁽²¹⁾ T. Maruyama,⁽²¹⁾
 A.K. McKemey,⁽³⁾ R. Messner,⁽²¹⁾ K.C. Moffeit,⁽²¹⁾ T.B. Moore,⁽³⁰⁾ M. Morii,⁽²¹⁾
 D. Muller,⁽²¹⁾ V. Murzin,⁽¹⁴⁾ S. Narita,⁽²⁴⁾ U. Nauenberg,⁽⁵⁾ H. Neal,⁽³⁰⁾ G. Nesom,⁽¹⁷⁾
 N. Oishi,⁽¹⁵⁾ D. Onoprienko,⁽²³⁾ L.S. Osborne,⁽¹³⁾ R.S. Panvini,⁽²⁷⁾ C.H. Park,⁽²²⁾
 I. Peruzzi,⁽⁸⁾ M. Piccolo,⁽⁸⁾ L. Piemontese,⁽⁷⁾ R.J. Plano,⁽²⁰⁾ R. Prepost,⁽²⁹⁾
 C.Y. Prescott,⁽²¹⁾ B.N. Ratcliff,⁽²¹⁾ J. Reidy,⁽¹²⁾ P.L. Reinertsen,⁽²⁶⁾ L.S. Rochester,⁽²¹⁾
 P.C. Rowson,⁽²¹⁾ J.J. Russell,⁽²¹⁾ O.H. Saxton,⁽²¹⁾ T. Schalk,⁽²⁶⁾ B.A. Schumm,⁽²⁶⁾
 J. Schwiening,⁽²¹⁾ V.V. Serbo,⁽²¹⁾ G. Shapiro,⁽¹⁰⁾ N.B. Sinev,⁽¹⁶⁾ J.A. Snyder,⁽³⁰⁾
 H. Staengle,⁽⁶⁾ A. Stahl,⁽²¹⁾ P. Stamer,⁽²⁰⁾ H. Steiner,⁽¹⁰⁾ D. Su,⁽²¹⁾ F. Suekane,⁽²⁴⁾
 A. Sugiyama,⁽¹⁵⁾ A. Suzuki,⁽¹⁵⁾ M. Swartz,⁽⁹⁾ F.E. Taylor,⁽¹³⁾ J. Thom,⁽²¹⁾ E. Torrence,⁽¹³⁾
 T. Usher,⁽²¹⁾ J. Va'vra,⁽²¹⁾ R. Verdier,⁽¹³⁾ D.L. Wagner,⁽⁵⁾ A.P. Waite,⁽²¹⁾ S. Walston,⁽¹⁶⁾
 A.W. Weidemann,⁽²³⁾ E.R. Weiss,⁽²⁸⁾ J.S. Whitaker,⁽⁴⁾ S.H. Williams,⁽²¹⁾ S. Willocq,⁽¹¹⁾
 R.J. Wilson,⁽⁶⁾ W.J. Wisniewski,⁽²¹⁾ J.L. Wittlin,⁽¹¹⁾ M. Woods,⁽²¹⁾ T.R. Wright,⁽²⁹⁾
 R.K. Yamamoto,⁽¹³⁾ J. Yashima,⁽²⁴⁾ S.J. Yellin,⁽²⁵⁾ C.C. Young,⁽²¹⁾ H. Yuta.⁽¹⁾

⁽¹⁾*Aomori University, Aomori, 030 Japan,*

⁽²⁾*University of Bristol, Bristol, United Kingdom,*

⁽³⁾*Brunel University, Uxbridge, Middlesex, UB8 3PH United Kingdom,*

⁽⁴⁾*Boston University, Boston, Massachusetts 02215,*

⁽⁵⁾*University of Colorado, Boulder, Colorado 80309,*

⁽⁶⁾*Colorado State University, Ft. Collins, Colorado 80523,*

⁽⁷⁾*INFN Sezione di Ferrara and Universita di Ferrara, I-44100 Ferrara, Italy,*

⁽⁸⁾*INFN Laboratori Nazionali di Frascati, I-00044 Frascati, Italy,*

⁽⁹⁾*Johns Hopkins University, Baltimore, Maryland 21218-2686,*

⁽¹⁰⁾*Lawrence Berkeley Laboratory, University of California, Berkeley, California 94720,*

⁽¹¹⁾*University of Massachusetts, Amherst, Massachusetts 01003,*

⁽¹²⁾*University of Mississippi, University, Mississippi 38677,*

⁽¹³⁾*Massachusetts Institute of Technology, Cambridge, Massachusetts 02139,*

⁽¹⁴⁾*Institute of Nuclear Physics, Moscow State University, 119899 Moscow, Russia,*

⁽¹⁵⁾*Nagoya University, Chikusa-ku, Nagoya, 464 Japan,*

⁽¹⁶⁾*University of Oregon, Eugene, Oregon 97403,*

⁽¹⁷⁾*Oxford University, Oxford, OX1 3RH, United Kingdom,*

⁽¹⁸⁾*INFN Sezione di Perugia and Universita di Perugia, I-06100 Perugia, Italy,*

- ⁽¹⁹⁾ *Rutherford Appleton Laboratory, Chilton, Didcot, Oxon OX11 0QX United Kingdom,*
⁽²⁰⁾ *Rutgers University, Piscataway, New Jersey 08855,*
⁽²¹⁾ *Stanford Linear Accelerator Center, Stanford University, Stanford, California 94309,*
⁽²²⁾ *Soongsil University, Seoul, Korea 156-743,*
⁽²³⁾ *University of Tennessee, Knoxville, Tennessee 37996,*
⁽²⁴⁾ *Tohoku University, Sendai, 980 Japan,*
⁽²⁵⁾ *University of California at Santa Barbara, Santa Barbara, California 93106,*
⁽²⁶⁾ *University of California at Santa Cruz, Santa Cruz, California 95064,*
⁽²⁷⁾ *Vanderbilt University, Nashville, Tennessee 37235,*
⁽²⁸⁾ *University of Washington, Seattle, Washington 98105,*
⁽²⁹⁾ *University of Wisconsin, Madison, Wisconsin 53706,*
⁽³⁰⁾ *Yale University, New Haven, Connecticut 06511.*

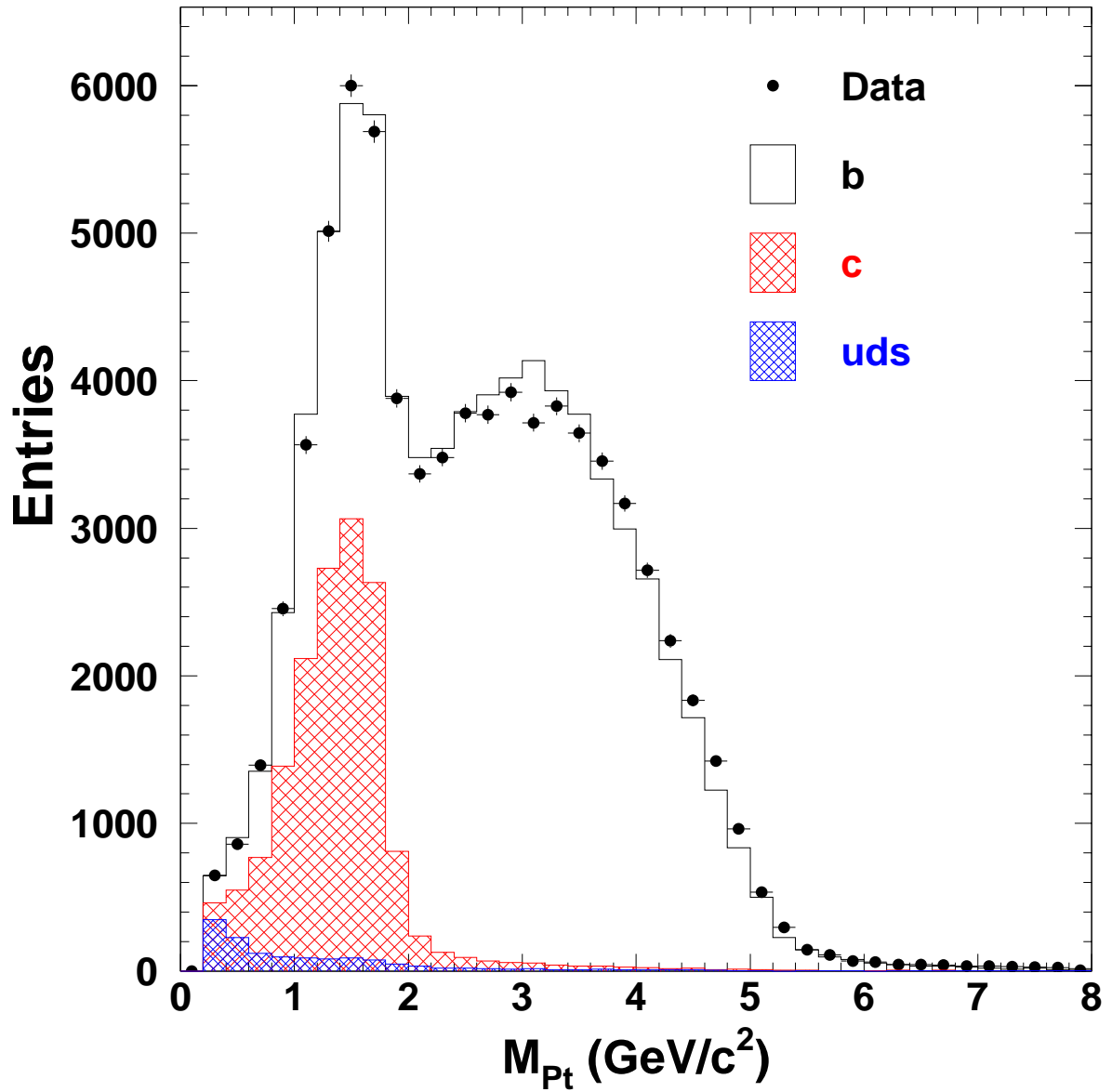


Figure 1: Distribution of the reconstructed P_t -corrected vertex mass in the 1997-98 data (points). Also shown is the prediction of the Monte Carlo simulation, for which the flavor composition is indicated: b (open), c (light shaded), and uds (dark shaded).

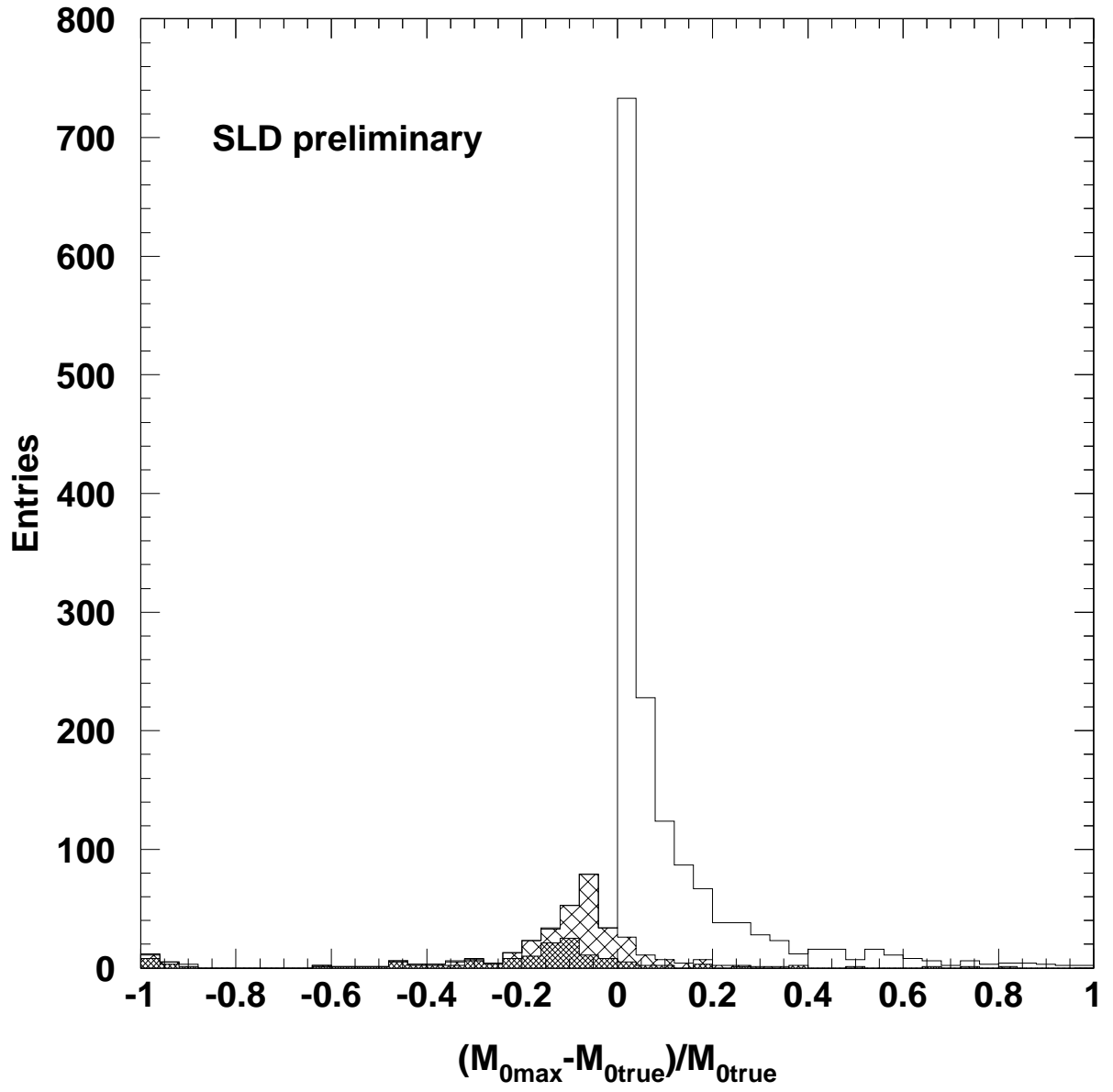


Figure 2: The relative deviation of the maximum missing mass from the true missing mass for Monte Carlo simulated B hadron decays, which is divided into three categories: B^0 and B^\pm (open), B_s^0 (cross-hatched), and Λ_b (dark hatched).

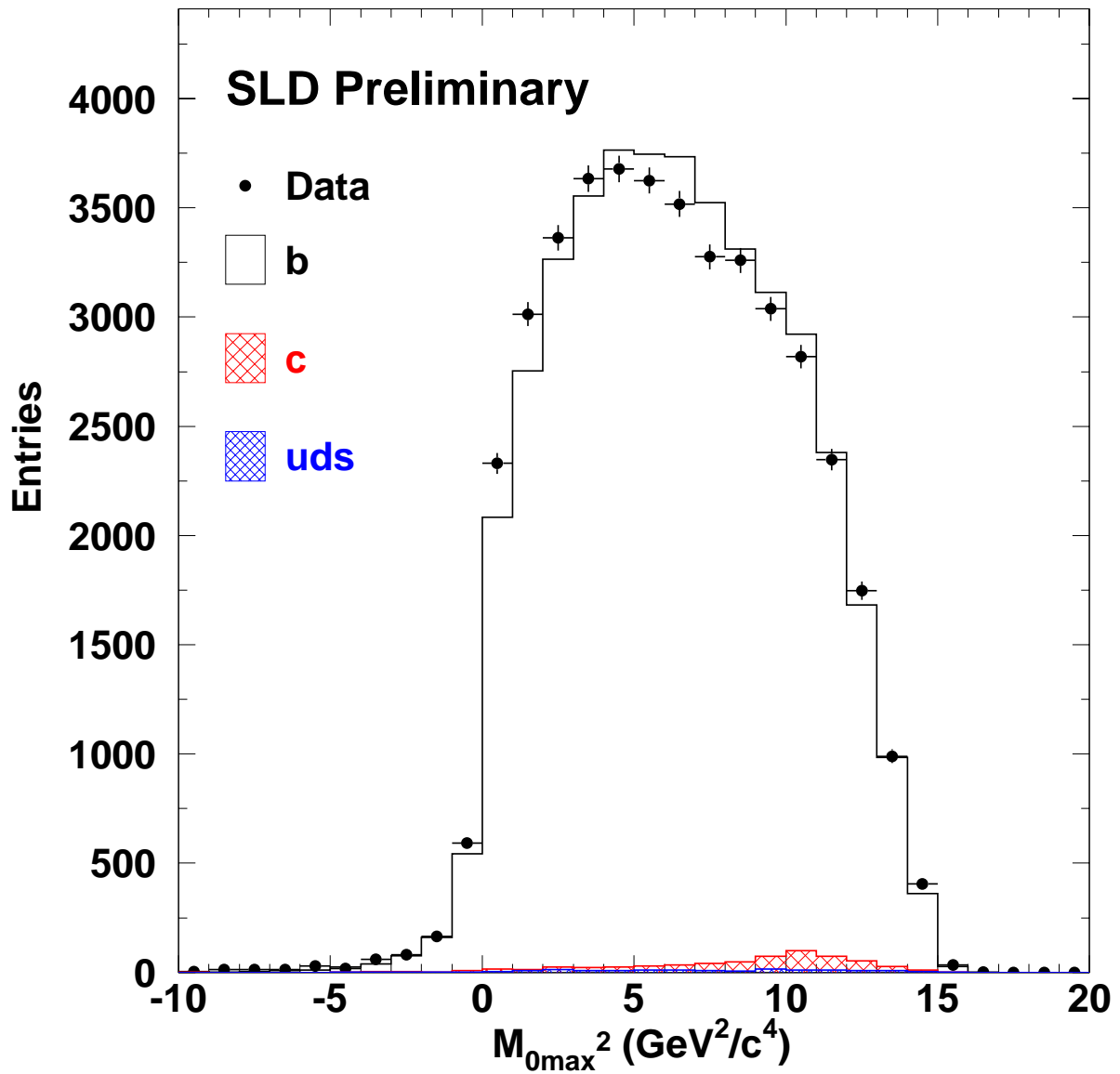


Figure 3: Distribution of the reconstructed M_{0max}^2 for the selected vertices in the 1997-98 data (points). Also shown is the prediction of the Monte Carlo simulation.

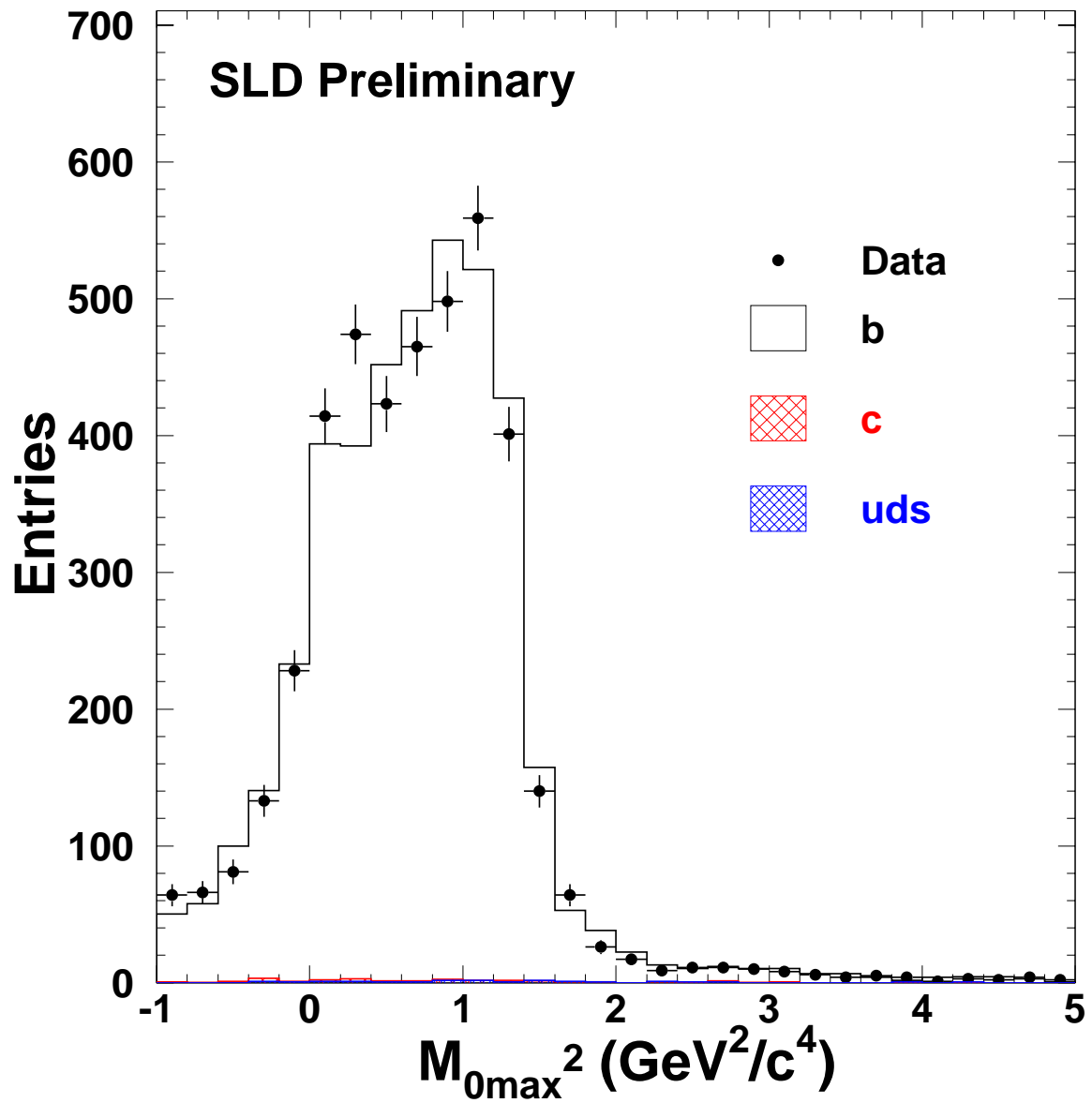


Figure 4: Distribution of the reconstructed M_{0max}^2 for the final selected B sample (see text). Also shown is the prediction of the Monte Carlo simulation.

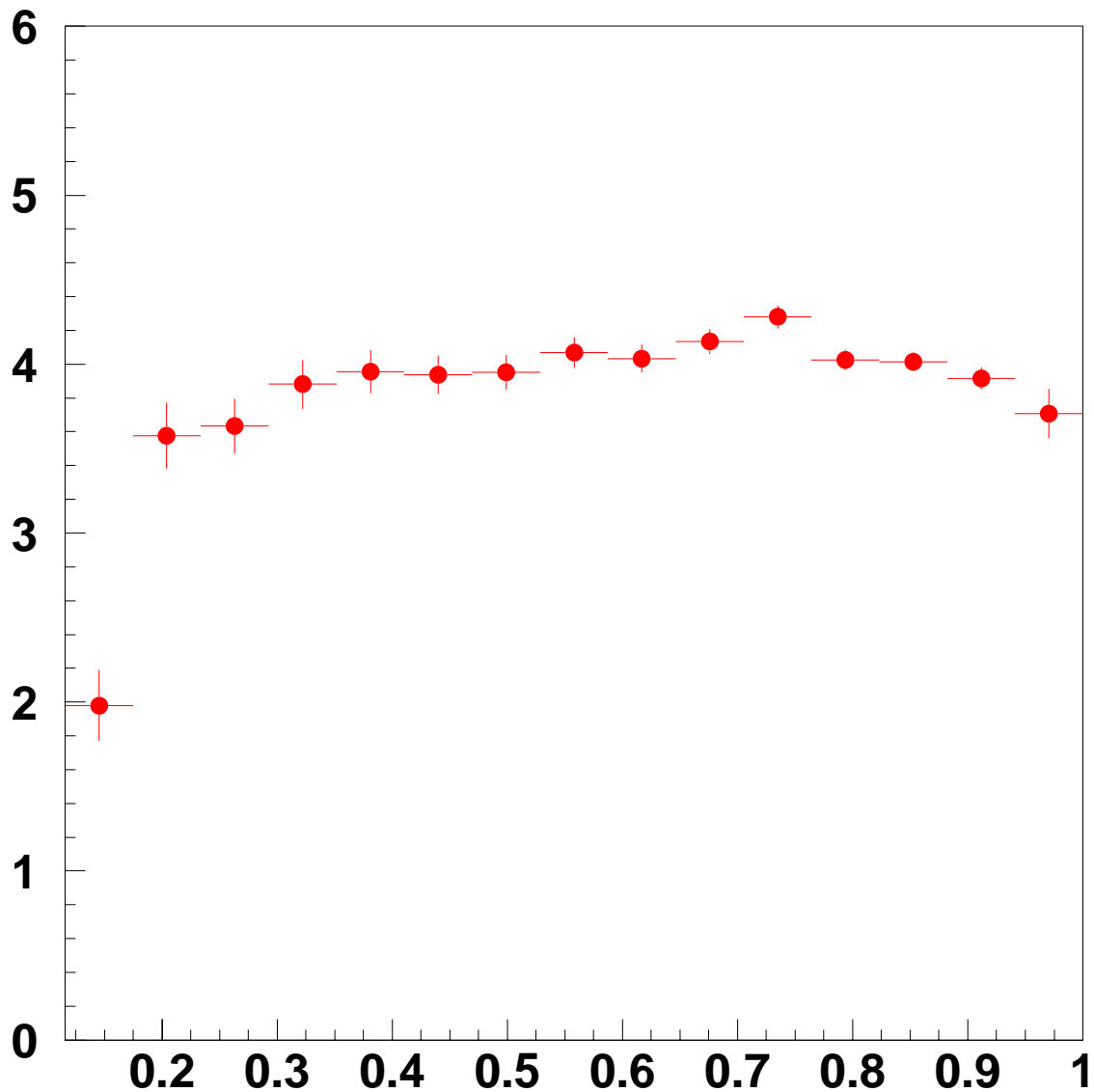


Figure 5: The Monte Carlo simulated efficiency for selecting B hadron decay vertices as a function of the true scaled B hadron energy, $x^{true} = E_B^{true}/E_{beam}$. The nearly energy-independent efficiency (except at very low B energy) improves the sensitivity of the measured x_B^{rec} distribution to the true underlying B energy distribution.

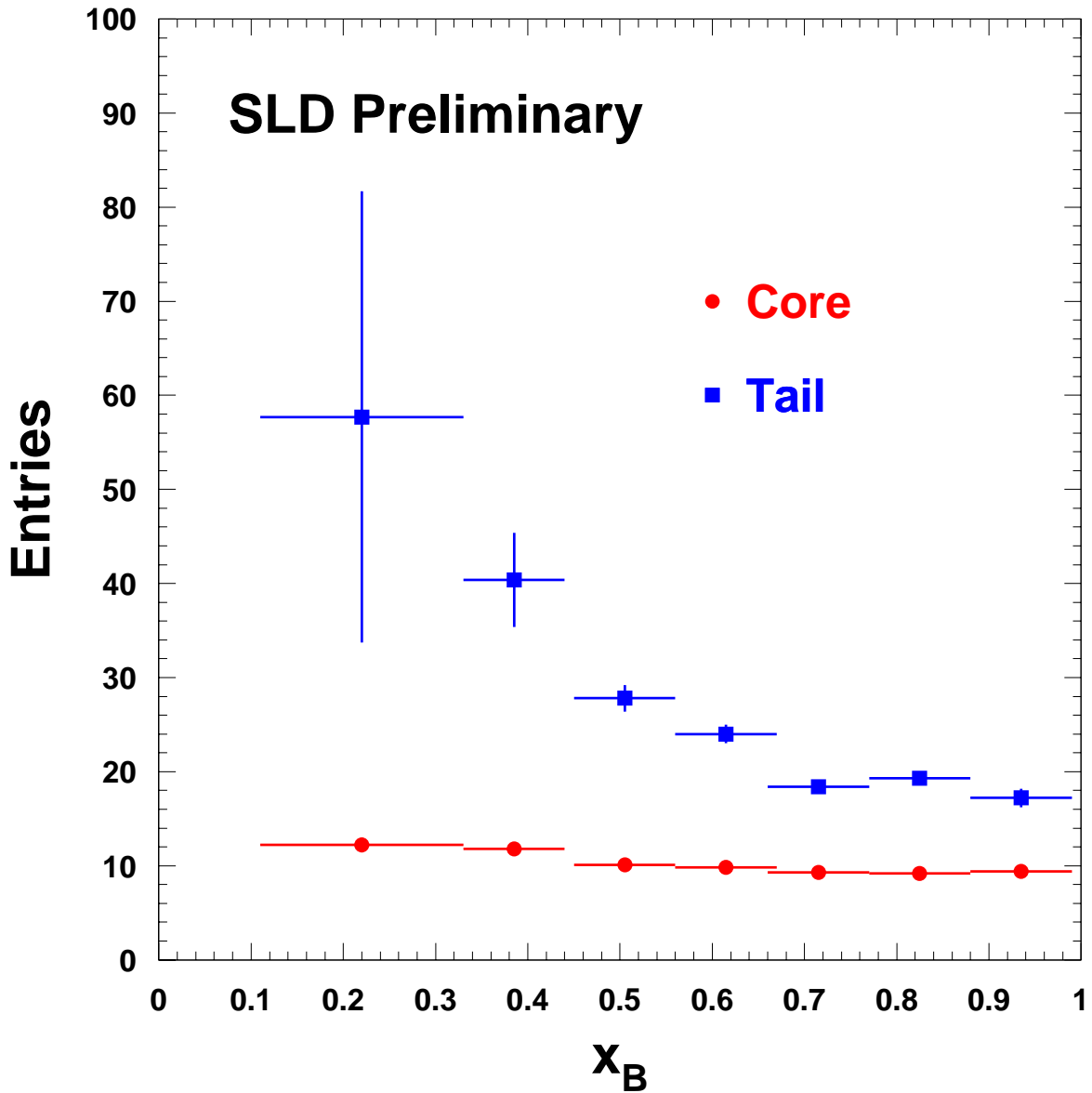


Figure 6: The fitted core and tail widths of the B energy resolution as a function of the true scaled B hadron energy. The ratio of the amplitude of the inner Gaussian (core) to that of the outer Gaussian (tail) is 84:16. The dependence of the core resolution on the true B energy is small. The very good resolution for low energy B hadrons improves the sensitivity of the measured x_B^{rec} distribution to the true underlying B energy distribution.

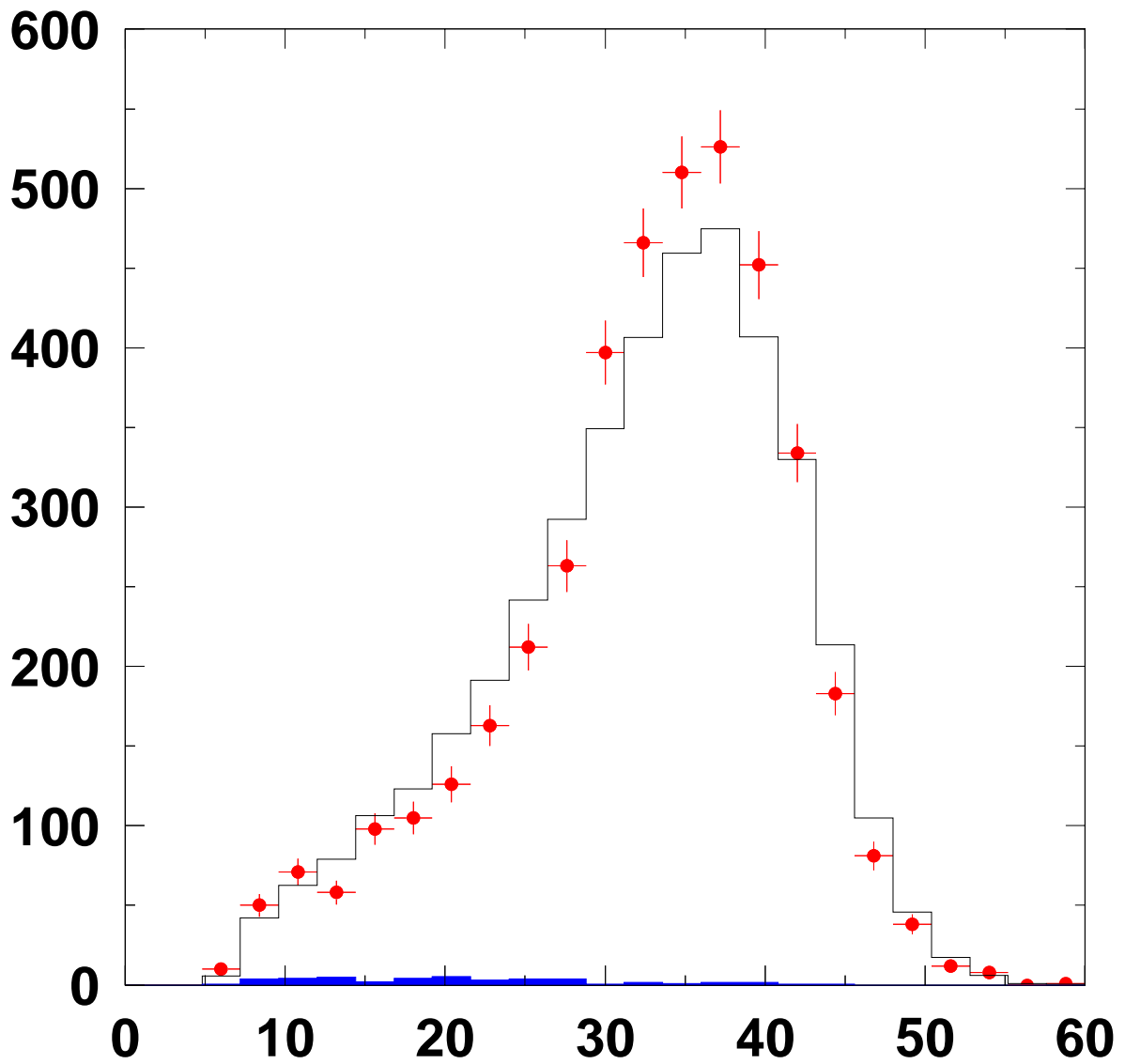


Figure 7: Distribution of the reconstructed B hadron energy for 1997-98 data (points) and the default Monte Carlo simulation (histogram). The solid histogram shows the simulated non- $b\bar{b}$ background.

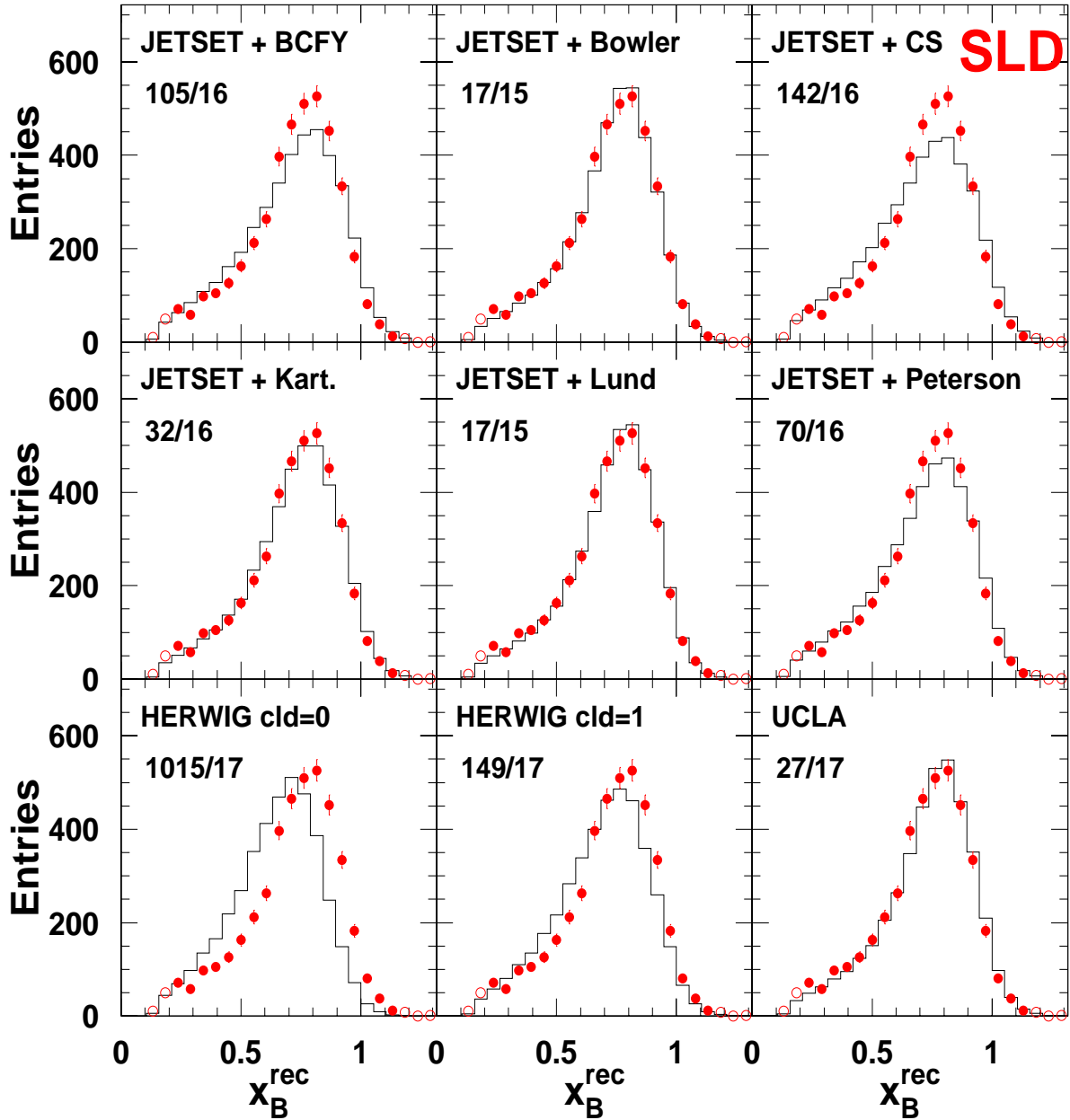


Figure 8: Each figure shows the background-subtracted distribution of reconstructed B hadron energy for the data (points) and for the Monte Carlo (histogram) based on the respective optimised input fragmentation function within the JETSET parton shower simulation, as well as based on the HERWIG ($cldir = 0$ and $cldir = 1$) and the UCLA fragmentation models. The χ^2 and the number of degrees of freedom are indicated.

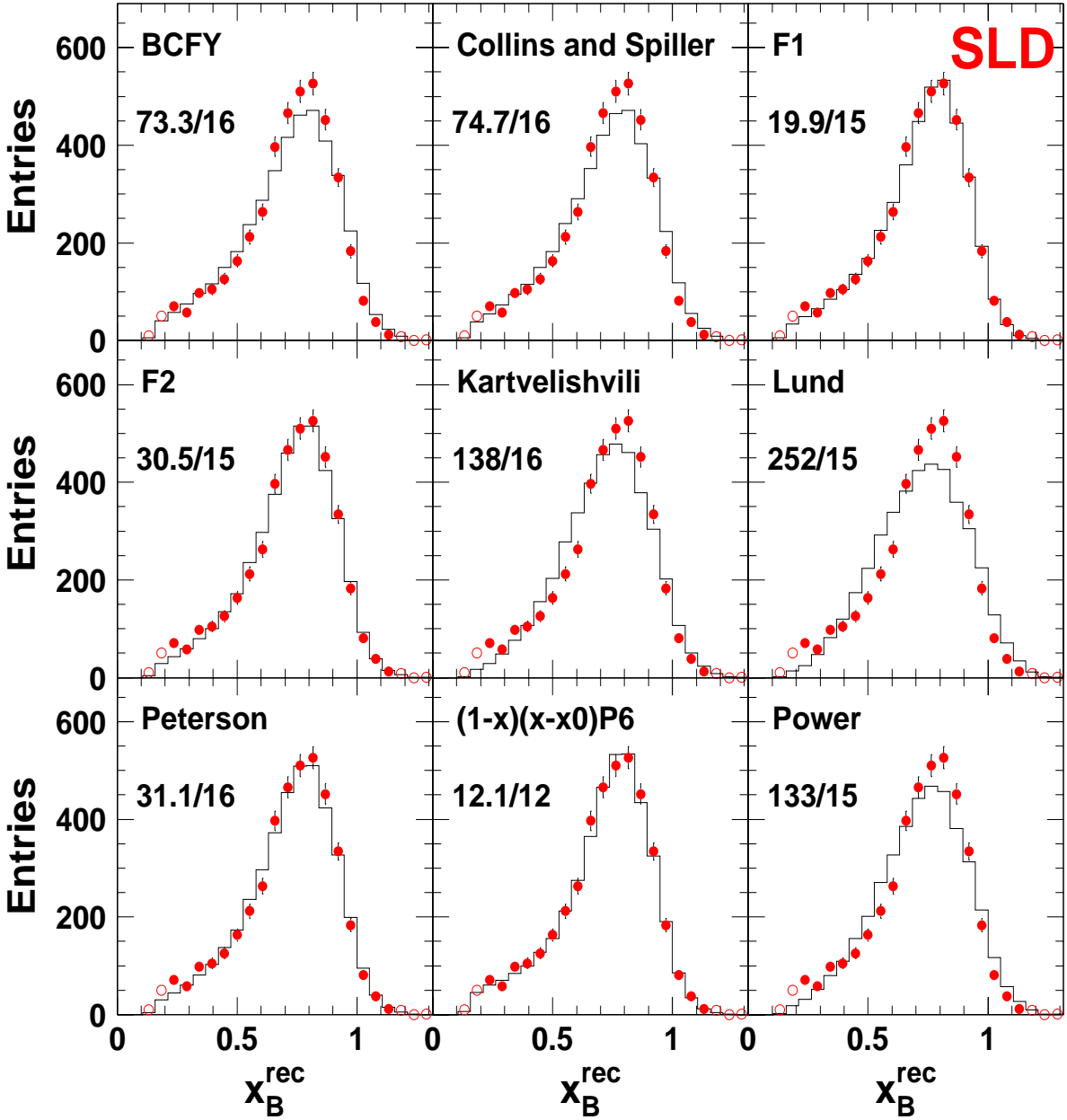


Figure 9: Each figure shows the background-subtracted distribution of reconstructed B hadron energy for the data (points) and for the weighted simulation (histograms) based on the respective optimised input functional form for the *true* B energy distribution. The χ^2 and the number of degrees of freedom are indicated.

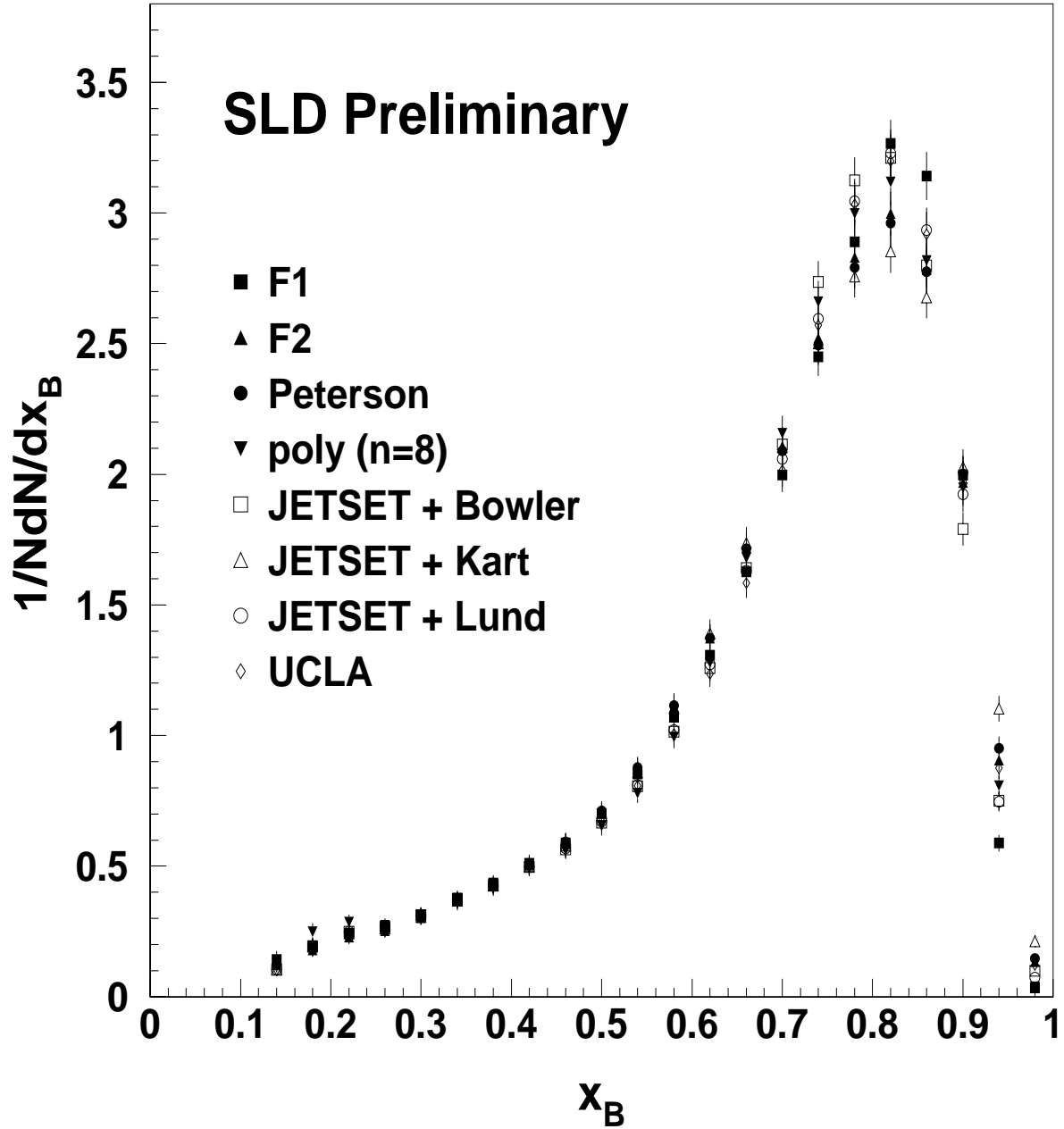


Figure 10: The efficiency-resolution corrected distributions of scaled weakly-decaying B hadron energies for **Case 1)** fragmentation models of the Lund, the Bowler and the Karvelishvili within the JETSET parton shower Monte Carlo as well as for the UCLA fragmentation model; and for **Case 2)** four functional forms: F1, F2, Peterson, and the constrained 8th-order polynomial.

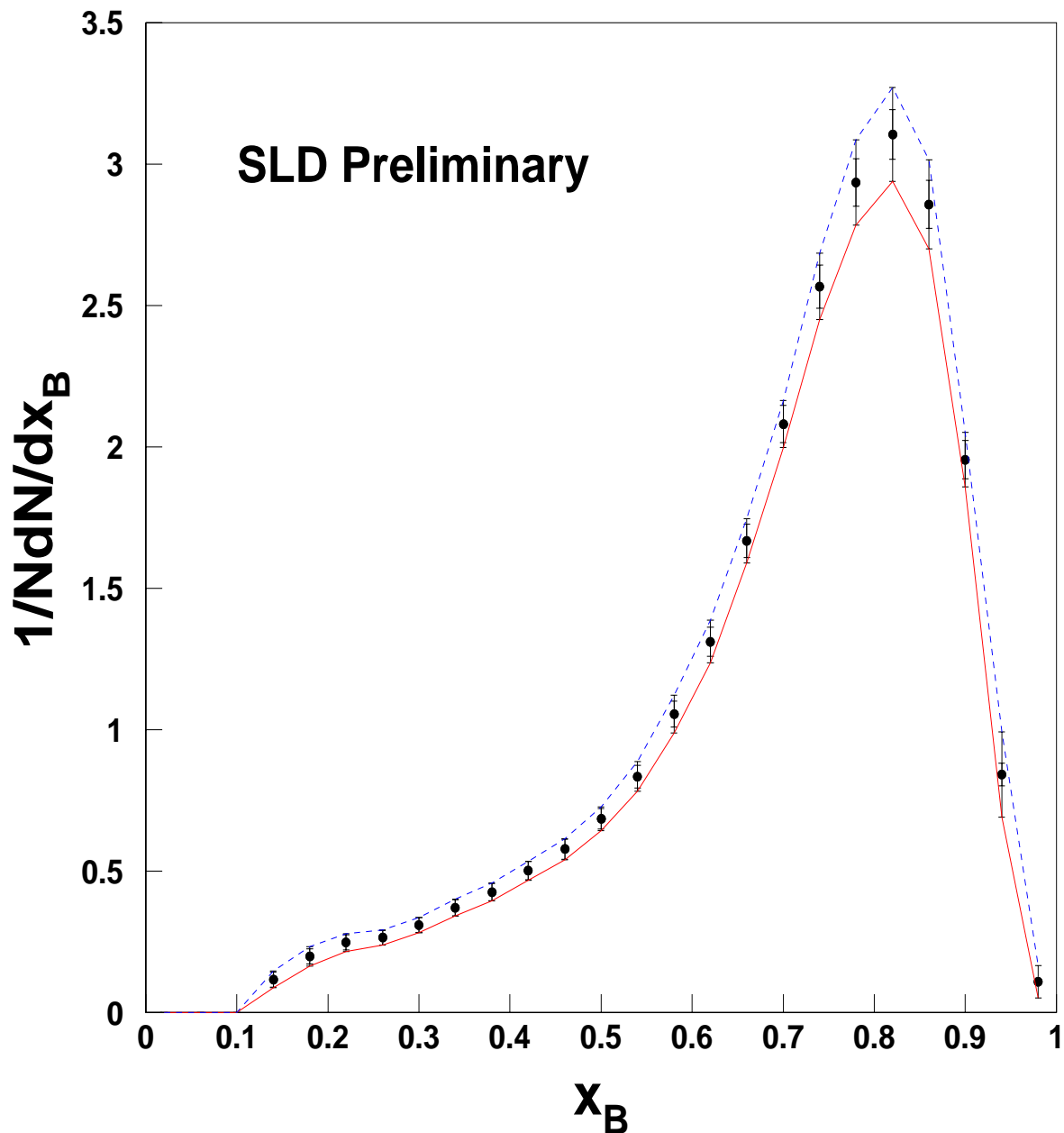


Figure 11: Distribution of the final corrected scaled B hadron energies. The central value is the bin-by-bin average of the eight consistent B energy distributions. In each bin the statistical error is indicated by the inner error bar, the sum in quadrature of statistical and unfolding errors from model dependence by the outer error bar. Systematic errors are small compared with the statistical and model dependence errors and are not included here. Note that the first two bins are below the kinematic limit for x_B (no point shown).

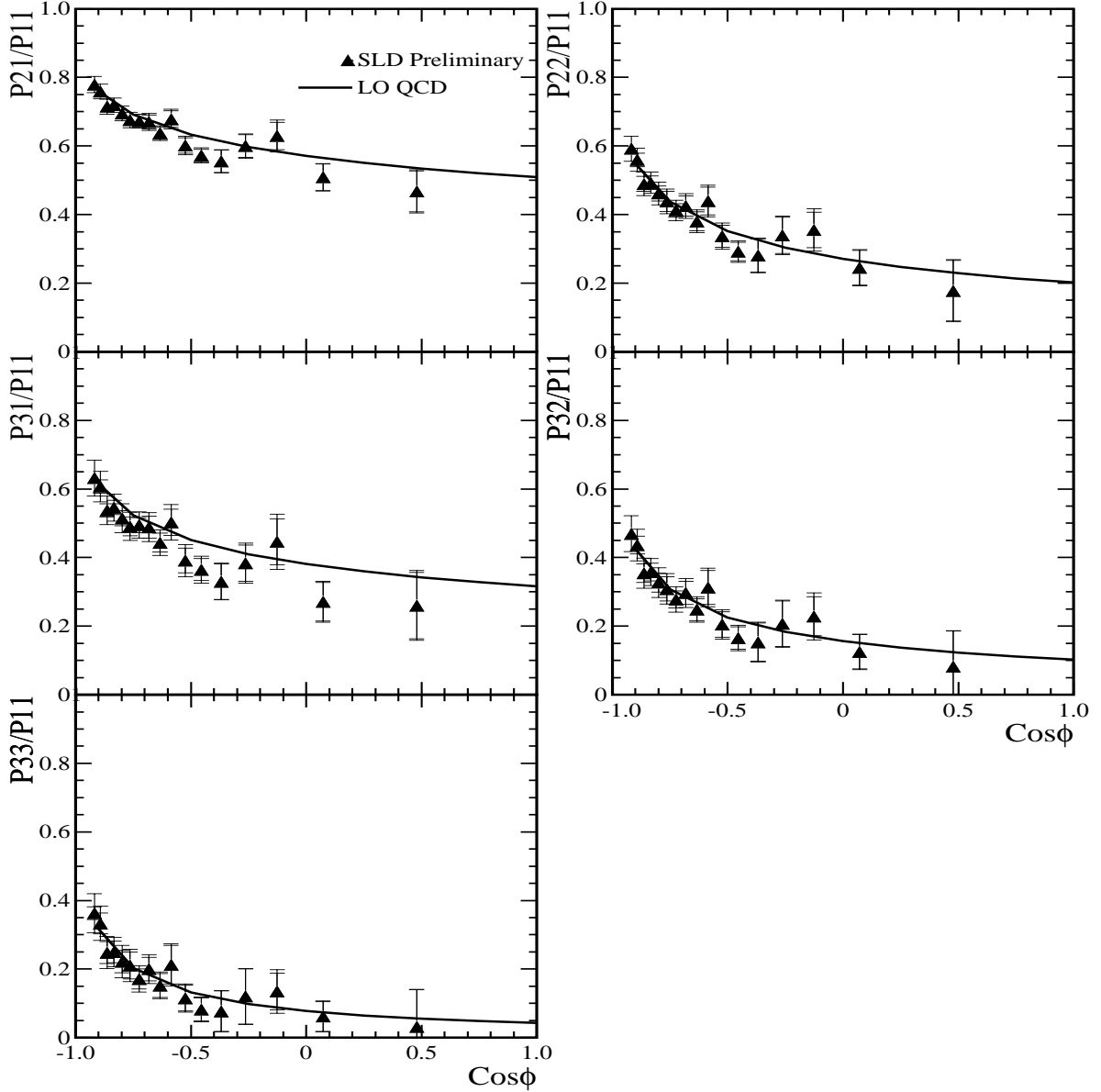


Figure 12: Ratio of moments P_{ij}/P_{11} (see text) vs. $\cos\phi$. Data: points with error bars; the inner error bar represents the statistical error and the outer error bar is the sum in quadrature of the statistical and systematic errors. The lines represent the LO QCD prediction (see text).